Pergamon

Geochimica et Cosmochimica Acta, Vol. 61, No. 9, pp. 1829–1846, 1997

0016-7037/97 $17.00 + .00

PII S0016-7037(97)00033-1

Partitioning of moderately siderophile elements among olivine, silicate melt, and sulfide melt: Constraints on core formation in the Earth and Mars

GLENN A. GAETANI* and TIMOTHY L. GROVE

Department of Earth, Atmospheric and Planetary Sciences, Massachusetts Institute of Technology, Cambridge, Massachusetts 02139, USA

(*Received May* 2, 1996; *accepted in revised form January* 14, 1997)

Abstract—This study investigates the effects of variations in the fugacities of oxygen and sulfur on the partitioning of first series transition metals (V, Cr, Mn, Fe, Co, Ni, and Cu) and W among coexisting sulfide melt, silicate melt, and olivine. Experiments were performed at 1 atm pressure, 1350°C, with the fugacities of oxygen and sulfur controlled by mixing CO_2, CO, and SO_2 gases. Starting compositions consisted of a CaO-MgO-Al_2O_3-SiO_2-FeO-Na_2O analog for a barred olivine chondrule from an ordinary chondrite and a synthetic komatiite. The f_{O_2}/f_{S_2} conditions ranged from log $f_{O_2} = -7.9$ to -10.6, with log f_{S_2} values ranging from -1.0 to -2.5. Our experimental results demonstrate that the f_{O_2}/f_{S_2} dependencies of sulfide melt/silicate melt partition coefficients for the first series transition metals are proportional to their valence states. The f_{O_2}/f_{S_2} dependencies for the partitioning of Fe, Co, Ni, and Cu are weaker than predicted on the basis of their valence states. Variations in f_{O_2}/f_{S_2} conditions have no significant effect on olivine/melt partitioning other than those resulting from f_{O_2}-induced changes in the valence state of a given element. The strong f_{O_2}/f_{S_2} dependence for the olivine/silicate melt partitioning of V is attributable to a change of valence state, from 4+ to 3+, with decreasing f_{O_2}. Our experimentally determined partition coefficients are used to develop models for the segregation of sulfide and metal from the silicate portion of the early Earth and the Shergottite parent body (Mars). We find that the influence of S is not sufficient to explain the overabundance of siderophile and chalcophile elements that remained in the mantle of the Earth following core formation. Important constraints on core formation in Mars are provided by our experimental determination of the partitioning of Cu between silicate and sulfide melts. When combined with existing estimates for siderophile element abundances in the Martian mantle and a mass balance constraint from Fe, the experiments allow a determination of the mass of the Martian core (~17 to 22 wt% of the planet) and its S content (~0.4 wt%). These modeling results indicate that Mars is depleted in S, and that its core is solid.

1. INTRODUCTION

The segregation of metallic cores from silicate mantles is the most significant differentiation event in the evolution of the terrestrial planets. In the Earth, for example, the inner and outer cores combined comprise ~33% of the mass of the planet. In contrast, the extraction of basalt from the upper mantle at mid-ocean ridges produces an oceanic crust comprising only ~0.08% of the mass of the Earth. The absolute and relative abundances of siderophile elements (elements that partition strongly into metallic phases relative to silicates) that remain in the silicate mantle of a planet following core formation provide the only direct geochemical evidence relating to the segregation process. These abundances should, in principle, reflect equilibration between metallic phases and mantle silicates during segregation of material into the core.

The conditions under which core formation took place could have had a significant effect on the present-day siderophile element abundance pattern of the mantle through variations in metal/silicate partitioning. The effects of such variables as temperature and pressure on siderophile element partitioning are beginning to be understood and quantified (Jones and Walker, 1991; Murthy, 1991; Keppler and Rubie, 1993; Walker et al., 1993; Capobianco and Amelin, 1994; Hillgren et al., 1994; Thibault and Walter, 1995; Li and Agee, 1996). In this study, we present experiments that investigate the effect of variations in the fugacities of oxygen (f_{O_2}) and sulfur (f_{S_2}) on the partitioning of moderately siderophile elements (V, Cr, Mn, Fe, Co, Ni, Cu, and W) among coexisting olivine, silicate melt, and sulfide melt. The experimental results are used to constrain the role of sulfide in producing the siderophile element abundance pattern in the upper mantle of the Earth and the conditions under which core formation took place in the parent body of Shergottite meteorites (Mars).

2. EXPERIMENTAL AND ANALYTICAL METHODS

Experiments were performed at 1 atm pressure in either a Pt-wound or Deltech vertical quenching furnace fitted with a 19 mm outer diameter fused-silica muffle tube. Fused silica was chosen to minimize interaction with the furnace gases, but had the disadvantage of needing to be replaced frequently. End-pieces were fabricated from fired pyrophyllite and attached to the muffle tube using General Electric Red RTV 106 high temperature silicone rubber adhesive sealant. The values of f_{O_2} and f_{S_2} were controlled by mixing CO_2, CO, and SO_2 gases that were fed into the furnace through a tube in the upper pyrophyllite plug (Fig. 1). The gases exited through a tube in the lower plug and were fed into a Pyrex flask through a silica-glass tube wrapped with heating tape, and then vented into a fume hood. Temperature in the furnace hotspot was continuously monitored using a Pt-$Pt_{90}Rh_{10}$ thermocouple calibrated against the

* *Present address:* Division of Geological and Planetary Sciences, California Institute of Technology, Pasadena, California 91125, USA.

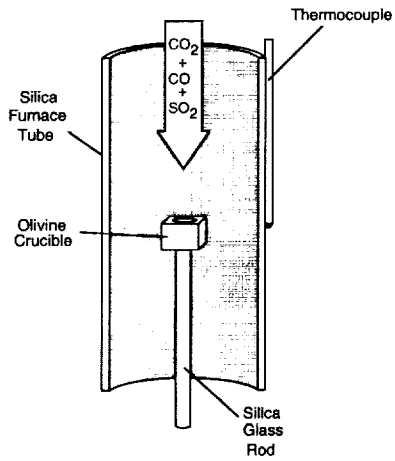

Fig. 1. Schematic of the furnace configuration used to perform the siderophile element partitioning experiments reported in this study.

melting points of NaCl, Au, and Pd on the 1968 International Practical Temperature Scale (Biggar, 1972). The thermocouple was positioned on the outside of the muffle tube to avoid contamination by S-rich gases, and the temperature difference between the position of the thermocouple and the position of the sample was calibrated using a second thermocouple.

The mixture of CO_2, CO, and SO_2 gases required for each experiment was calculated by assuming that the gas behaves as an ideal solution at high temperature and low pressure and is given in Table 1. Expressions relating Gibbs free energy change to equilibrium constants for independent reactions involving nine gas species (O_2, CO, CO_2, COS, CS_2, S_2, SO, SO_2, SO_3) were written using thermochemical data from the JANAF tables (Chase et al., 1985). Mass balance equations relating each element (C, O, and S) to the stable gas species were then used to determine the gas mixture necessary to achieve the desired combination of f_{O_2} and f_{S_2}. This calculation procedure gives results that are in agreement with those determined using the method of steepest descent, a calculation procedure based on free energy minimization that has been used in other experimental studies involving CO_2-CO-SO_2 gas mixing (White et al., 1958; Haughton et al., 1974).

Starting materials consisted of either a CaO-MgO-Al_2O_3-SiO_2-FeO-Na_2O analog for a barred olivine chondrule from an ordinary chondrite (Fo86 of Ehlers et al., 1992) or a synthetic Munro Township komatiite (KOM; Composition B of Kinzler and Grove, 1985) (Table 2) to which synthetic FeS and various combinations of Johnson-Matthey high-purity NiO, CuO, Cr_2O_3, Co_3O_4, V_2O_5, or WO_3 were added (Table 1). FeS was synthesized by melting a 2 gram stoichiometric mixture of Fe metal sponge and S chips in an evacuated silica-glass tube. The tube containing the FeS mixture was placed in a Deltech vertical quenching furnace at 960°C; the temperature was raised gradually to 1250°C over a period of 2 h, then quickly to 1270°C and held at that temperature for 2 h before quenching the charge into water.

Experiments were performed by packing the sample powder into a crucible fabricated from a single crystal of gem quality San Carlos olivine (Fo_{89-91}) following the methods described by Ehlers et al. (1992). Olivine crucibles are preferable to containers made from high-purity alumina because they prevent reaction between the crucible and charge during olivine-saturated melting experiments. The crucible was fastened to the top of a silica-glass rod using 0.2 mm diameter Pt wire and placed into the furnace through the lower end of the muffle tube with the hotspot temperature set to 1078°C. The lower pyrophyllite plug was then used to seal the furnace tube and the gases were set to the desired flow rates. After the gases had been flowing for 30 min, the sample was raised into the hotspot. A second glass rod was placed between the benchtop and the rod holding the sample, and the hotspot temperature was gradually raised to 1350°C over a period of ~60 min. At the end of each experiment the lower glass rod was removed and the upper rod slid down, quenching the experiment against the lower pyrophyllite plug. This method of quenching resulted in little or no quench growth in the silicate glass, but the sulfide melt generally consisted of a coarse intergrowth of quench phases, a common problem in experiments containing sulfide melts (e.g., Jones and Drake, 1983; Jones and Walker, 1991; Peach and Mathez, 1993). Evidence for the loss of Cu from the charges due to volatilization was found in one experiment performed at relatively oxidizing conditions ($\log f_{O_2} = -7.9$; $\log f_{S_2} = -2.0$; gas flow rate of 1.29 mL/s). This problem was minimized in other experiments through the use of low gas flow rates and deep crucibles.

Experimental products were analyzed using either a 4- or 5-spectrometer JEOL 733 Superprobe at the Massachusetts Institute of Technology. Analytical conditions for determination of the major elements in all phases were an accelerating voltage of 15 kV and a beam current of 10 nA with maximum peak counting times of 40 s. A 1 μm spot size was used for analyses of olivine and sulfide, while a 10 μm spot size was used to perform glass analyses. Each reported silicate analysis represents a mean of 10 spot analyses. On-line data reduction was accomplished using the phi-rho-z correction scheme. Trace elements in the silicate phases were analyzed separately from the major elements using a beam current of 200 nA and peak counting times ranging from 250–700 s, depending on concentration. Elements present in the sulfide melt in trace amounts were analyzed using beam currents of 50–200 nA and peak counting times of 250–500 s, depending on concentration. The detection limit for trace elements was taken to be 3 standard deviations above background counts. Analyzing experiments containing V required corrections for peak overlap interferences from $Ti_{K\beta}$ on $V_{K\alpha}$ and $V_{K\beta}$ on $Cr_{K\alpha}$. This was accomplished by determining the intensity of the interfering peak on the pure oxide of the interfering element (i.e., TiO_2 and V_2O_5) and then scaling the interference for a given analysis to the concentration of the interfering element and subtracting it from the measured intensity of the element of interest.

The olivine/silicate melt partition coefficients for Cu were determined by secondary ion mass spectrometry using the Cameca IMS 3f ion microprobe at Woods Hole Oceanographic Institution. Analyses were performed using a 2 nA beam of O^- ions focused to a spot size of 15 μm. Positive secondary ions were collected and counted by an electron multiplier. Molecular interferences were excluded by energy filtering using a ±10-V energy window and a −90V offset (Shimizu and Hart, 1982), and checked by determining the $^{63}Cu/^{65}Cu$ ratio for each spot. The relationships between intensity and concentration for olivine and glass were determined using experiment KOM-1s, in which the concentration of Cu in olivine is high enough to be determined by electron microprobe.

Accurate determinations of the compositions of experimentally produced sulfide melts were complicated by the presence of coarse intergrowths of quench phases. This problem has been dealt with in other studies by performing multiple broad-beam analyses (Peach and Mathez, 1993), or by rastering the beam over large areas (Walker et al., 1993). Our approach to this problem was to analyze each quench phase separately, to use image analysis to determine their relative proportions, and then to calculate a weighted mean composition for the bulk sulfide melt. The uncertainty associated with the quench phase proportions was estimated by performing replicate determinations and calculating the standard deviation of the mean for each quench phase.

3. EXPERIMENTAL RESULTS

3.1. Synthesis Experiments

Experiments were performed on a synthetic Munro Township komatiite composition (KOM) (Table 2) to determine the partitioning behavior of V, Cr, Mn, Fe, Co, Ni, Cu, and W among coexisting olivine, sulfide melt, and ultramafic silicate melt. The partitioning behavior of Ni was also experimentally determined for the CaO-MgO-Al_2O_3-SiO_2-FeO-Na_2O barred olivine chondrule analog composition (Fo86; Table 2) studied by Ehlers et al. (1992). The komatiite provides a reasonable analog for the type of high-degree partial melt that might be present if the silicate portion of a

TABLE 1. Experimental conditions and phase assemblages for partitioning experiments.

Experiment	Duration (hr)	log f_{O_2}	log f_{S_2}	Gas Flow Rates (mL/s) $CO_2 : CO : SO_2$	Run Products
Ni-Doped Experiments					
Fo86-8s[1]	48	−7.9	−2.5	1.53 : 0.41 : 0.11	Gl, Oliv, Slf
Fo86-5s[1]	49	−7.9	−2.0	0.95 : 0.30 : 0.15	Gl, Oliv, Slf
Fo86-9s[1]	48	−8.0	−1.5	0.51 : 0.30 : 0.18	Gl, Oliv, Slf, PrEn
Fo86-15s[1]	49	−8.6	−1.5	0.39 : 0.39 : 0.08	Gl, Oliv, Slf, PrEn
Fo86-14s[1]	48	−9.4	−1.5	0.27 : 0.71 : 0.08	Gl, Oliv, Slf, PrEn
Fo86-10s[1]	48	−10.3	−1.5	0.08 : 1.44 : 0.12	Gl, Oliv, Slf, PrEn
Ni-Cr-Cu-Doped Experiments					
KOM-1s[2]	48	−7.9	−1.8	0.46 : 0.17 : 0.10	Gl, Oliv, Sp, Slf
KOM-6s[2]	48	−8.0	−1.5	0.51 : 0.30 : 0.18	Gl, Oliv, Sp, Slf
KOM-15s[3]	72	−8.8	−1.5	0.50 : 0.61 : 0.10	Gl, Oliv, Sp, Slf
KOM-4s[2]	48	−9.2	−1.0	0.00 : 0.77 : 0.20	Gl, Oliv, Sp[10], Slf
KOM-3s[2]	48	−10.3	−1.5	0.08 : 1.44 : 0.12	Gl, Oliv, Sp[10], Slf
KOM-10s[4]	72	−10.3	−1.5	0.10 : 1.66 : 0.13	Gl, Oliv, Sp[10], Slf
KOM-26s[4,9]	72	−7.9	−2.0	0.87 : 0.28 : 0.14	
	72	−10.3	−1.5	0.10 : 1.66 : 0.13	Gl, Oliv, Sp[10], Slf
KOM-9s[4]	72	−10.6	−1.5	0.00 : 1.28 : 0.10	Gl, Oliv, Sp[10], Slf
Ni-Co-W-Doped Experiments					
KOM-16s[5]	72	−7.9	−1.8	0.46 : 0.17 : 0.10	Gl, Oliv, Sp, Slf
KOM-20s[5]	72	−8.0	−1.5	0.51 : 0.30 : 0.18	Gl, Oliv, Sp, Slf
KOM-13s[6]	72	−9.4	−1.5	0.27 : 0.71 : 0.08	Gl, Oliv, Sp[10], Slf, (Tngst?)
KOM-11s[6]	72	−10.3	−1.5	0.08 : 1.44 : 0.12	Gl, Oliv, Sp[10], Slf, Tngst
Ni-V-Doped Experiments					
KOM-19s[7]	72	−7.9	−1.8	0.46 : 0.17 : 0.10	Gl, Oliv, Sp, Slf
KOM-23s[7]	74	−8.0	−1.5	0.51 : 0.30 : 0.18	Gl, Oliv, Sp, Slf
KOM-22s[7]	90	−9.1	−1.5	0.44 : 0.78 : 0.10	Gl, Oliv, Sp[10], Slf
KOM-18s[8]	72	−10.3	−1.5	0.08 : 1.44 : 0.12	Gl, Oliv, Sp[10], Slf

Abbreviations: Gl = glass, Oliv = olivine; Slf = sulfide; PrEn = protoenstatite; Sp = spinel; Tngst = tungstate mineral.
[1]Doped with 1.5 wt% NiO; 1.5 wt% FeS.
[2]Doped with 1.5 wt% NiO; 1.5 wt% FeS; 1.0 wt% CuO.
[3]Doped with 1.5 wt% NiO; 1.5 wt% FeS; 1.0 wt% CuO, 1 wt% Cr_2O_3.
[4]Doped with 2.5 wt% NiO; 1.5 wt% FeS; 2.0 wt% CuO, 1 wt% Cr_2O_3.
[5]Doped with 1.5 wt% NiO; 1.5 wt% FeS; 1.0 wt% Co_3O_4, 1 wt% WO_3.
[6]Doped with 2.5 wt% NiO; 1.5 wt% FeS; 1.0 wt% Co_3O_4, 1 wt% WO_3.
[7]Doped with 1.5 wt% NiO; 1.5 wt% FeS; 1 wt% V_2O_5.
[8]Doped with 3.5 wt% NiO; 1.5 wt% FeS; 1 wt% V_2O_5.
[9]Reversal experiment.
[10]Spinel occurs within sulfide melt.

terrestrial planet were largely molten (e.g., Nisbet and Walker, 1982). The Fo86 experiments allow the partitioning behavior of Ni in a S-bearing system to be directly compared with the results of Ehlers et al. (1992), who performed Ni-partitioning experiments in a S-free system using the Fo86 composition. Experimental conditions were log f_{O_2} values ranging from −7.9 (1 log unit more reduced than the fayalite-magnetite-quartz, FMQ, oxygen buffer) to −10.6 (the iron-quartz-fayalite, IQF, oxygen buffer) and log f_{S_2} values from −1.0 to −2.5 (Table 1; Fig. 2). At 1350°C both starting compositions produce silicate melts saturated with an immiscible sulfide melt and olivine. In addition, the KOM experiments crystallize chromian spinel, while protoenstatite occurs in the Fo86 experiments performed at low f_{O_2}/f_{S_2} ratio conditions (Table 1). The KOM experiments containing W that were performed at reducing conditions also contain a tungstate mineral.

Olivine grains in the KOM experiments are subhedral to euhedral in morphology, tend to be elongate, and are up to ~600 μm in their long dimension (Fig. 3). Spinels occur as small (~5–20 μm), equant, euhedral grains. In the high f_{O_2}/f_{S_2} ratio experiments spinel is present in the silicate melt and included in olivine grains, while in the low f_{O_2}/f_{S_2} ratio experiments it occurs exclusively within the sulfide melt (Table 1). The tungstate mineral occurs as small (~5 μm), spheroidal grains within the sulfide melt. The morphology of the sulfide melt changes dramatically with varying f_{O_2}/f_{S_2} experimental conditions. In the high f_{O_2}/f_{S_2} ratio experiments, the sulfide melt is present as small (~10 μm) to moderate size (~250 μm) spheres throughout the upper portion of the charge. In the low f_{O_2}/f_{S_2} ratio experiments the sulfide melt forms large (~1,500 μm), lens-shaped bodies that commonly occur at the silicate melt/gas interface (Fig. 3).

TABLE 2. Compositions (wt%) of silicate starting materials.

	SiO_2	TiO_2	Al_2O_3	Cr_2O_3	FeO	MnO	MgO	CaO	Na_2O	K_2O	NiO	Total
Fo86	47.94	—	7.13	—	8.94	—	31.40	1.39	3.19	—	—	99.99
KOM	50.14	0.33	10.55	0.41	10.98	0.36	17.21	9.49	0.37	0.07	0.09	100.00

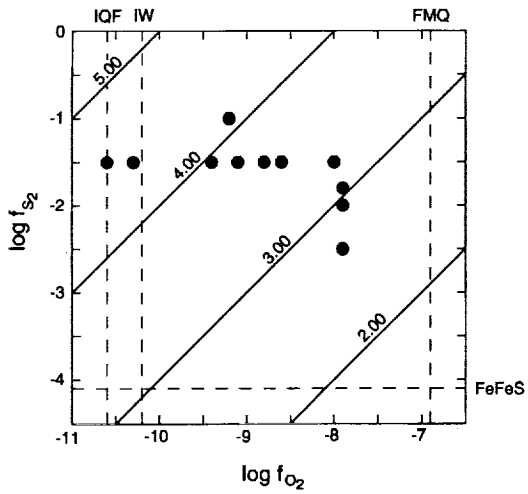

Fig. 2. Plot of log f_{O_2} versus log f_{S_2} showing conditions at which siderophile element partitioning experiments were performed (filled circles). Diagonal solid lines represent constant log $f_{S_2}^{1/2}$ − log $f_{O_2}^{1/2}$ values. Vertical dashed lines represent the iron-quartz-fayalite (IQF), iron-wüstite (IW), and fayalite-magnetite-quartz (FMQ) oxygen buffers at 1350°C. Horizontal dashed line represents the iron-iron sulfide (FeFeS) sulfur buffer at 1350°C.

Olivine grains in the Fo86 experiments are subhedral to euhedral in morphology, and tend to be equant. The largest grains are typically 40–60 μm in diameter. Sulfide occurs as spherical to sub-spherical blebs, up to 110 μm in diameter, distributed throughout the silicate melt. Pyroxene grains are subhedral to euhedral and tend to be elongate. The largest grains are up to ~700 μm in length. In the experiments where olivine and pyroxene coexist, there is a distinct trend of increasing protoenstatite and decreasing olivine abundance with decreasing f_{O_2}/f_{S_2} ratio. There is also a decrease in the total number of crystals with decreasing f_{O_2}/f_{S_2} ratio.

The composition of the silicate melt varies systematically with changing f_{O_2}/f_{S_2} ratio for both starting compositions. The abundances of FeO, NiO, CuO, and CoO all decrease with decreasing f_{O_2}/f_{S_2} ratio, while the abundance of dissolved S increases (Tables 3–6). The decrease in FeO produces a corresponding increase in the concentration of the other major elements. This compositional variation leads to low-Ca pyroxene saturation in the Fo86 experiments performed at low f_{O_2}/f_{S_2} ratio conditions.

The composition of the sulfide melt also varies as the f_{O_2}/f_{S_2} ratio decreases. The sulfide melt in the high f_{O_2}/f_{S_2} ratio experiments is Ni-rich, while in the low f_{O_2}/f_{S_2} experiments it is Fe-rich (Table 7; Fig. 4). The concentrations of V, Cr, and Mn in the sulfide melt increase with decreasing f_{O_2}/f_{S_2} ratio. In contrast with the other first series transition metals, the abundances of Cu and Co do not vary in a systematic way. In the case of Cu, this may be related to the need to use higher doping levels to obtain accurate microprobe analyses of experiments performed at low f_{O_2}/f_{S_2} ratio conditions (see footnotes in Table 1 for the doping levels used in each experiment). The sulfur contents of the sulfide melts range from 28.8 to 38.3 wt%, and increase systematically with decreasing f_{O_2}/f_{S_2} ratio (Table 7).

The weight ratio sulfide melt/silicate melt partition coefficients ($D_M^{\text{Sulfide Melt/Silicate Melt}}$ = [wt% M in sulfide melt]/[wt% M in silicate melt]) for all of the elements studied (with the possible exception of W) are strong functions of the f_{O_2}/f_{S_2} ratio (Tables 8–9; Fig. 5). The weight ratio olivine/silicate partition coefficients ($D_M^{\text{Olivine/Silicate Melt}}$ = [wt% M in olivine]/[wt% M in silicate melt]) for Ni, Mn, Cr, and Cu do not show a systematic variation with changing f_{O_2}/f_{S_2} conditions, while those for V and W increase with decreasing f_{O_2}/f_{S_2} ratio (Table 10; Fig. 6). The Co partition coefficients are similar to those determined in a S-free systems by Ehlers et al. (1992) for the Fo86 composition.

Olivine/silicate melt partition coefficients for Ni are within 2 standard deviations of the values predicted by the model of Kinzler et al. (1990) in the experiments performed at conditions more oxidizing than the iron-wüstite solid oxygen buffer (IW), as is the case in the S-free system (Ehlers et al., 1992). The olivine/silicate melt partition coefficient in the Fo86 experiment performed at conditions slightly more reducing than IW is 4.0 ± 0.4, significantly lower than the value predicted on the basis of the compositions of the coexisting olivine and melt (7.1 ± 0.9), but similar to the values reported by Ehlers et al. (1992) at comparable f_{O_2} conditions.

3.2. Approach to Equilibrium

The approach to equilibrium represented by our experiments was determined through (1) reproducibility of partition coefficients in different experiments performed at the same conditions, (2) comparison of the olivine/melt $K_D^{Fe/Mg}$ for olivine that crystallized directly from the melt with that for the olivine crucible adjacent to the melt, and (3) a reversal experiment.

Multiple experiments were carried out at log f_{O_2} = −7.9, log f_{S_2} = −1.8 (KOM-1s; -16s; -19s), at log f_{O_2} = −8.0, log f_{S_2} = −1.5 (KOM-6s; -20s; -23s), and at log f_{O_2} = −10.9, log f_{S_2} = −1.5 (KOM-3s; -10s; -11s; -18s) (Table 1). The sulfide melt/silicate melt partition coefficients for Ni measured in KOM-1s (540 ± 10) and KOM-16s (510 ± 10) overlap at the 2σ level, but that measured in KOM-19s (410 ± 20) is low. This apparent discrepancy may reflect an underestimation of the uncertainty associated with the image analysis procedure used to determine the proportions of the quench phases. There is good agreement among the sulfide melt/silicate melt partition coefficients for Ni (550 ± 10; 580 ± 30; 550 ± 20) and Mn (0.06 ± 0.03; 0.07 ± 0.01) measured at log f_{O_2} = −8.0, log f_{S_2} = −1.5. The same is true in the log f_{O_2} = −10.3, log f_{S_2} = −1.5 experiments for Ni (3600 ± 200; 4400 ± 400; 3800 ± 400). The sulfide melt/silicate melt partition coefficients for Mn in experiments KOM-10s (1.07 ± 0.05), KOM-11s (1.09 ± 0.03), and KOM-18s (0.94 ± 0.04) are similar, but the Mn partition coefficient determined from KOM-3s (1.49 ± 0.04) is high. The sulfide melt/silicate melt partition coefficients for Cr agree in KOM-10s (4.8 ± 0.2) and KOM-18s (4.9 ± 0.2). There is also agreement between KOM-3s (7.2 ± 0.3) and KOM-11s (6.3 ± 0.5). Although the pairs of partition coefficients are similar, they do not overlap at the 2σ level.

Equilibration of the crucible with the melt is an important prerequisite for equilibration of the entire charge. Table 11 demonstrates that there is good agreement between the compositions of the olivine

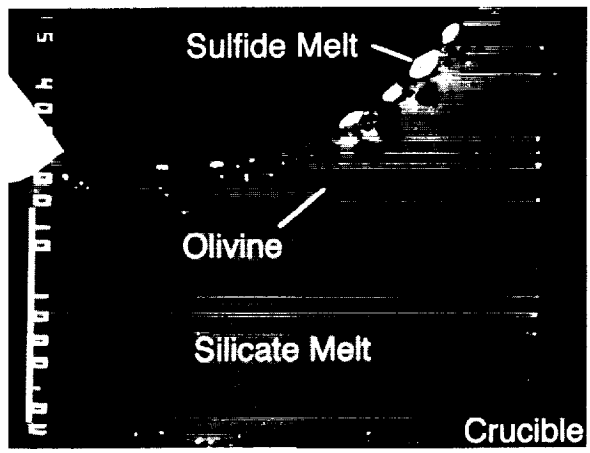

Fig. 3. Backscattered electron image showing a cross section through a siderophile element partitioning experiment performed at f_{O_2} conditions near IW. Co-existing phases are silicate melt, sulfide melt, and olivine. Experiment was performed at 1 atm, 1350°C, in a crucible fabricated from San Carlos olivine. Scale bar is 1000 μm.

TABLE 3. Electron microprobe analyses of silicate phases from experiments performed on Ni-doped Fo86 starting composition.

Experiment	Phase	SiO_2	Al_2O_3	FeO*	MgO	CaO	Na_2O	NiO	S	Total
Fo86-8s	Gl	60.9(8)	11.3(2)	9.1(4)	13.5(7)	2.5(1)	2.4(2)	0.130(9)	0.031(3)	99.86
	Oliv	40.5(4)	0.05(2)	9.7(2)	49.2(5)	0.04(1)	—	0.97(4)	—	100.46
Fo86-5s	Gl	61.6(3)	11.7(1)	7.9(2)	13.2(2)	2.34(6)	3.2(3)	0.116(3)	0.028(1)	100.08
	Oliv	40.7(3)	0.08(2)	9.5(1)	49.5(3)	0.04(2)	—	0.84(2)	—	100.66
Fo86-9s	Gl	60.8(4)	11.5(1)	8.6(1)	14.6(1)	2.32(3)	2.5(1)	0.091(7)	0.041(4)	100.45
	Oliv	40.5(2)	0.1(2)	9.7(1)	49.8(5)	0.05(2)	—	0.59(2)	—	100.74
Fo86-15s	Gl	59.5(3)	13.2(2)	8.2(2)	14.4(1)	2.62(6)	2.76(6)	0.040(4)	0.047(5)	100.77
	Oliv	40.7(3)	0.03(1)	8.9(1)	50.6(5)	0.05(1)	—	0.28(2)	—	100.56
Fo86-14s	Gl	59.6(2)	14.9(1)	6.8(1)	13.6(1)	3.1(1)	2.61(7)	0.017(2)	0.060(1)	100.69
	Oliv	41.3(3)	0.04(2)	7.9(1)	51.1(4)	0.05(1)	—	0.120(5)	—	100.51
Fo86-10s	Gl	59.1(7)	16.5(2)	3.2(2)	16.0(4)	3.2(1)	2.3(1)	0.007(2)	0.080(2)	100.39
	Oliv	41.8(3)	0.07(1)	3.68(7)	54.9(4)	0.06(1)	—	0.028(3)	—	100.54

Notes: Units in parentheses represent 1 standard deviation of least units cited on the basis of replicate analyses; thus, 60.9(8) should be read as 60.9±0.8. Abbreviations as in Table 1.

that crystallized from the komatiite melt and the olivine crucible within a few μm of the silicate melt. This indicates that although Fe/Mg exchange was necessary for the crucible to achieve equilibrium with the silicate melt over the range of f_{O_2}/f_{S_2} conditions investigated, a close approach to equilibrium was achieved during each experiment.

A reversal of equilibrium was attempted by performing an experiment at log $f_{O_2} = -7.9$, log $f_{S_2} = -1.5$ for 72 h, then changing the gas flow rates to achieve log $f_{O_2} = -10.3$, log $f_{S_2} = -1.5$ and continuing the experiment for an additional 72 h. The run products from this experiment consist of glass, olivine, sulfide, and spinel. The abundance and morphology of the phases are identical to those found in synthesis experiments, with the sole exception of the presence of spinel inclusions in some of the olivine grains. The presence of these inclusions is an indication that their host olivine grew at the initial conditions of the experiment, during which spinel occurred in the silicate melt and as inclusions in olivine grains. Analyses of the cores of these grains ($Fo_{96.4\pm0.2}$), which are 110 to 145 μm in diameter, are in good agreement with the composition of the rims and the crucible adjacent to the glass (Table 11), indicating reequilibration. The sulfide melt/silicate melt partition coefficients for Cr (4.8 ± 0.2 versus 4.9 ± 0.2), Mn (1.07 ± 0.05 versus 0.99 ± 0.05), and Cu (900 ± 100 versus 670 ± 70) in KOM-10s and the reversal experiment overlap at the 2σ level. The partition coefficient for Ni in the reversal experiment is low (2400 ± 300) relative to that in KOM-10s (3600 ± 200), but they overlap at 2.4σ. Once again, this may reflect an underestimation of the uncertainty associated with determining the proportions of the sulfide quench phases using image analysis.

4. DISCUSSION

4.1. Effect of Variable f_{O_2} and f_{S_2} on Siderophile Element Partitioning

Explicit dependence of sulfide melt/silicate melt partitioning on f_{O_2} and f_{S_2} is governed by an exchange reaction of the form:

$$M_X O_Y^{\text{Silicate Melt}} + \frac{Z}{2} S_2^{\text{Gas}} = M_X S_Z^{\text{Sulfide Melt}} + \frac{Y}{2} O_2^{\text{Gas}} \quad (1)$$

where M is a metal cation and X, Y, and Z are stoichiometric coefficients. An increase in f_{S_2} at a constant f_{O_2} value (i.e., a decrease in the f_{O_2}/f_{S_2} ratio) will drive this reaction to the product side, increasing the sulfide melt/silicate melt partition coefficient, while an increase in f_{O_2} at a constant f_{S_2} will favor the reactants, leading to a decrease in the sulfide melt/silicate melt partition coefficient (e.g., Peach and Mathez, 1993). This relationship can be quantified by rewriting Eqn. 1 in terms of a single metal cation:

$$MO_{Y/X}^{\text{Silicate Melt}} + \frac{Z}{2X} S_2^{\text{Gas}} = MS_{Z/X}^{\text{Sulfide Melt}} + \frac{Y}{2X} O_2^{\text{Gas}} \quad (2)$$

TABLE 4. Electron microprobe analyses of silicate phases from experiments performed on KOM starting composition doped with Cr, Ni, and Cu.

Experiment	Phase	SiO_2	TiO_2	Al_2O_3	Cr_2O_3	FeO	MnO	MgO	CaO	Na_2O	K_2O	NiO	CuO	S	Total
KOM-1s	Gl	51.4(3)	0.38(2)	10.9(1)	0.246(3)	11.2(2)	0.314(2)	15.2(1)	10.0(1)	0.23(4)	0.06(1)	0.086(2)	0.073(3)	0.065(2)	100.15
	Oliv	39.7(3)	—	0.07(1)	0.158(3)	10.89(9)	0.266(4)	47.8(3)	0.23(2)	—	—	0.58(1)	0.007(2)	—	99.69
KOM-6s	Gl	51.5(1)	0.35(2)	10.53(8)	0.371(3)	11.2(1)	0.296(2)	17.19(9)	9.33(9)	0.12(2)	0.02(1)	0.096(2)	0.026(2)	0.081(2)	101.11
	Oliv	40.3(1)	—	0.07(3)	0.22(1)	9.7(1)	0.225(2)	49.2(2)	0.23(1)	—	—	0.551(3)	—	—	100.50
KOM-15s	Gl	51.5(2)	0.34(2)	10.47(5)	0.530(3)	9.4(1)	0.300(4)	17.65(6)	9.32(6)	0.08(1)	0.01(0)	0.024(2)	0.011(2)	0.131(1)	99.77
	Oliv	40.4(2)	—	0.12(2)	0.324(5)	8.44(7)	0.214(3)	49.8(3)	0.21(1)	—	—	0.134(5)	—	—	99.64
KOM-4s	Gl	53.6(1)	0.35(2)	11.0(1)	0.271(1)	6.8(2)	0.322(4)	18.4(1)	9.84(5)	0.11(2)	0.01(1)	0.010(1)	0.011(2)	0.140(2)	100.86
	Oliv	41.3(2)	—	0.04(2)	0.178(5)	6.1(3)	0.230(2)	52.5(4)	0.21(1)	—	—	0.062(4)	—	—	100.62
KOM-3s	Gl	55.5(2)	0.36(2)	11.4(1)	0.222(1)	3.72(6)	0.311(3)	18.38(6)	10.3(1)	0.17(2)	0.03(1)	—	0.0086(5)[1]	0.154(3)	100.56
	Oliv	41.9(4)	—	0.03(1)	0.140(1)	3.55(6)	0.220(2)	54.6(7)	0.22(1)	—	—	0.017(1)	—		100.68
KOM-10s	Gl	55.5(2)	0.33(1)	11.22(6)	0.672(3)	4.2(1)	0.289(2)	18.3(1)	9.77(8)	0.05(1)	0.00	0.0043(8)	0.010(2)	0.140(3)	100.49
	Oliv	41.6(2)	—	0.08(2)	0.429(4)	3.81(7)	0.200(2)	54.4(2)	0.19(1)	—	—	0.030(6)	—	—	100.74
KOM-26s	Gl	55.0(1)	0.34(2)	11.54(8)	0.716(2)	4.09(8)	0.301(2)	18.41(9)	9.9(1)	0.07(2)	0.01(0)	0.007(2)	0.012(2)	0.133(5)	100.53
	Oliv	41.7(3)	—	0.07(2)	0.458(5)	3.70(9)	0.205(2)	54.4(3)	0.22(2)	—	—	0.045(7)	—	—	100.80
KOM-9s	Gl	56.1(2)	0.34(2)	11.23(4)	0.561(3)	2.94(5)	0.263(2)	19.3(1)	9.92(4)	0.08(2)	0.01(0)	—	0.012(2)	0.151(2)	100.91
	Oliv	42.1(2)	—	0.07(2)	0.354(3)	2.54(5)	0.179(2)	55.7(2)	0.21(1)	—	—	0.017(2)	—	—	101.17

Notes: Units in parentheses as in Table 2. Abbreviations as in Table 1.
[1]Determined by ion microprobe.

TABLE 5. Electron microprobe analyses of silicate phases from experiments on KOM starting composition doped with Co, Ni, and W.

Experiment	Phase	SiO_2	TiO_2	Al_2O_3	Cr_2O_3	FeO	MnO	MgO	CaO	Na_2O	K_2O	NiO	CoO	WO_3	S	Total
KOM-16s	Gl	49.1(2)	0.35(2)	10.59(7)	0.226(5)	11.7(2)	0.279(5)	16.0(1)	9.03(4)	0.13(2)	0.02(1)	0.121(3)	0.48(2)	1.03(2)	0.064(2)	99.12
	Oliv	39.8(2)	—	0.07(0)	0.13(1)	11.2(2)	0.191(9)	46.2(2)	0.22(2)	—	—	0.67(9)	0.87(8)	0.016(3)	—	99.37
KOM-20s	Gl	50.4(1)	0.35(2)	10.67(8)	0.254(2)	11.1(1)	0.297(3)	16.9(1)	9.23(9)	0.05(2)	0.00(1)	0.079(2)	0.435(2)	0.973(8)	0.08(1)	100.82
	Oliv	40.5(2)	—	0.09(1)	0.151(2)	9.68(9)	0.217(4)	49.0(2)	0.22(1)	—	—	0.45(1)	0.85(1)	0.052(5)	—	101.21
KOM-13s	Gl	51.9(3)	0.34(2)	10.6(1)	0.213(3)	8.2(2)	0.286(2)	17.71(8)	9.35(6)	0.05(1)	0.01(1)	0.018(2)	0.136(3)	0.71(2)	0.136(9)	99.66
	Oliv	41.0(2)	—	0.04(2)	0.134(3)	7.6(1)	0.205(4)	50.9(2)	0.20(1)	—	—	0.097(2)	0.263(5)	0.028(5)	—	100.47
KOM-11s	Gl	55.0(1)	0.37(2)	11.1(3)	0.163(1)	3.7(1)	0.285(2)	18.7(1)	9.8(1)	0.04(2)	0.01(1)	0.0034(9)	0.0357(6)	0.669(7)	0.141(2)	100.02
	Oliv	41.9(2)	—	0.03(2)	0.107(2)	3.39(6)	0.200(2)	54.5(2)	0.19(2)	—	—	0.024(3)	0.070(2)	0.036(6)	—	100.45

Notes: Units in parentheses as in Table 2. Abbreviations as in Table 1.

The equilibrium constant for this reaction is given by:

$$K_{eq} = \frac{a^{\text{Sulfide}}_{MS_{Z/X}} f^{Y/2X}_{O_2}}{a^{\text{Silicate}}_{MO_{Y/X}} f^{Z/2X}_{S_2}} \quad (3)$$

Taking logarithms and rearranging gives:

$$\log \frac{a^{\text{Sulfide}}_{MS_{Z/X}}}{a^{\text{Silicate}}_{MO_{Y/X}}} = \log f^{Z/2X}_{S_2} - \log f^{Y/2X}_{O_2} + \log K_{eq} \quad (4)$$

If the ratio of the activity coefficients for the M species in the silicate and sulfide melts remains constant over the range of f_{O_2}/f_{S_2} conditions of interest, it can be combined with the equilibrium constant and a molar-to-weight-ratio conversion factor to form a single constant term. Then, if $Y = Z$, Eqn. 4 can be simplified to give the expression:

$$\log D_M^{\text{Sulfide Melt/Silicate Melt}} = \frac{Y}{X}[\log f^{1/2}_{S_2} - \log f^{1/2}_{O_2}] + C \quad (5)$$

Therefore, if all of the appropriate assumptions are met, a linear relationship will exist between $\log D_M^{\text{Sulfide Melt/Silicate Melt}}$ and $\log f^{1/2}_{S_2} - \log f^{1/2}_{O_2}$ with a slope that is equal to the anion-to-cation ratio for the oxide or sulfide species of interest. The strength of the f_{O_2}/f_{S_2} dependence for a given element should be proportional to its valence state.

Figure 5 is a plot of $\log D_M^{\text{Sulfide Melt/Silicate Melt}}$ versus $\log f^{1/2}_{S_2} - \log f^{1/2}_{O_2}$ showing the partition coefficients determined from our experiments on the synthetic komatiite composition. The partition coefficient for W has been omitted because it could only be determined for a single experiment. The logarithms of the partition coefficients for all of the elements studied are strong linear functions of $\log f^{1/2}_{S_2} - \log f^{1/2}_{O_2}$, as expected. The slopes of the best-fit regression lines steepen from 0.38 ± 0.06 for Cu to 1.37 ± 0.08 for Cr (Table 8). The elements Fe, Co, Ni, and Cu are chalcophile ($D_M^{\text{Sulfide Melt/Silicate Melt}} > 1.0$) at all of the f_{O_2}/f_{S_2} conditions investigated. The elements V, Cr, and Mn go from being incompatible in the sulfide melt at high f_{O_2}/f_{S_2} ratios to being compatible at low f_{O_2}/f_{S_2} conditions. Due to the difference in their slopes, the partition coefficients for Mn and V reach a crossover point at $\log f^{1/2}_{S_2} - \log f^{1/2}_{O_2} = 4.35$, where V goes from being less compatible than Mn to being more compatible (Fig. 5). There is a similar crossover involving Fe and Cr at $\log f^{1/2}_{S_2} - \log f^{1/2}_{O_2} = 5.04$.

The relationship between the f_{O_2}/f_{S_2} dependence of sulfide melt/silicate melt partitioning and anion-to-cation ratio means that any change in the valence state of an element will complicate the linear relationship given by Eqn. 5. The advantage of partitioning among three coexisting phases is that any change in the valence state of an element with varying f_{O_2}/f_{S_2} conditions inferred from sulfide melt/silicate melt partitioning should also be reflected in the olivine/silicate melt partitioning data, providing an independent check. Unlike sulfide melt/silicate melt partitioning, olivine/silicate melt partitioning of moderately siderophile elements is not governed by an exchange reaction involving S and, therefore, should be largely insensitive to variations in f_{S_2}. A significant and systematic change in olivine/silicate melt partitioning with varying f_{O_2}/f_{S_2} conditions should, therefore, indicate a change in valence state related to changing f_{O_2} conditions. The olivine/silicate melt partition coefficients for Cr, Mn, Ni, Co, and Cu do not vary systematically with changing f_{O_2}/f_{S_2} conditions. The small amount of variability that does exist may be attributable to changes in the compositions of the coexisting olivine and silicate melt (e.g., Hart and Davis, 1978; Kinzler et al., 1990; Hirschmann and Ghiorso, 1994). Of these four elements, Cr and Mn have

TABLE 6. Electron microprobe analyses of silicate phases from experiments performed on KOM starting composition doped with V and Ni.

Experiment	Phase	SiO_2	TiO_2	Al_2O_3	Cr_2O_3	FeO	MnO	MgO	CaO	Na_2O	K_2O	NiO	V_2O_5	S	Total
KOM-19s	Gl	50.0(2)	0.346(3)	10.6(1)	0.240(2)	11.4(2)	0.288(3)	16.6(1)	9.37(7)	0.14(3)	0.03(1)	0.176(3)	1.00(1)	0.062(3)	100.25
	Oliv	40.1(3)	0.005(1)	0.07(0)	0.148(3)	10.0(2)	0.212(2)	47.9(3)	0.24(2)	—	—	1.05(2)	0.096(3)	—	99.82
KOM-23s	Gl	49.6(2)	0.347(3)	10.64(9)	0.250(2)	11.9(2)	0.293(3)	17.2(1)	8.81(7)	0.15(2)	0.02(1)	0.095(3)	1.048(5)	0.101(6)	100.45
	Oliv	40.4(2)	0.004(1)	0.06(2)	0.145(2)	10.2(1)	0.217(2)	48.7(2)	0.22(2)	—	—	0.52(2)	0.104(2)	—	100.57
KOM-22s	Gl	51.3(2)	0.356(4)	10.7(1)	0.247(6)	9.9(2)	0.303(5)	17.9(1)	9.17(6)	0.06(1)	0.01(1)	0.027(5)	0.99(1)	0.145(3)	101.11
	Oliv	40.8(2)	0.0047(7)	0.07(2)	0.147(1)	8.9(1)	0.216(3)	50.4(2)	0.21(1)	—	—	0.152(4)	0.157(2)	—	101.06
KOM-18s	Gl	55.0(2)	0.367(2)	11.15(8)	0.162(2)	3.87(7)	0.290(2)	18.64(8)	9.9(1)	0.09(2)	0.02(1)	0.006(1)	0.811(5)	0.153(1)	100.45
	Oliv	41.6(3)	0.0062(8)	0.06(2)	0.105(2)	3.4(1)	0.205(2)	54.3(2)	0.19(2)	—	—	0.027(2)	0.276(1)	—	100.17

Notes: Units in parentheses as in Table 2. Abbreviations as in Table 1.

TABLE 7. Electron microprobe analyses of experimentally-produced sulfide melts.

Experiment	Fe	Ni	Cu	Cr	Mn	Co	W	V	S	Total
Ni-Doped Experiments										
Fo86-8s[1]	13.3(3)	58.6(3)	—	—	—	—	—	—	28.8(2)	100.7
Fo86-5s	14.9(3)	56.3(8)	—	—	—	—	—	—	29.6(2)	100.8
Fo86-9s	21.9(6)	46.5(6)	—	—	—	—	—	—	31.3(1)	99.7
Fo86-15s	42.2(12)	24.0(9)	—	—	—	—	—	—	34.7(3)	100.9
Fo86-14s	43.9(5)	21.8(4)	—	—	—	—	—	—	33.9(3)	99.6
Fo86-10s[1]	50.7(8)	11.2(6)	—	—	—	—	—	—	38.3(5)	100.2
Ni-Cr-Cu-Doped Experiments										
KOM-1s	19.9(2)	36.4(2)	14.8(2)	—[2]	—[2]	—	—	—	30.0(1)	101.10
KOM-6s	20.9(5)	41.6(7)	6.5(1)	0.034(8)	0.013(8)	—	—	—	31.7(3)	100.75
KOM-15s	36.7(7)	21.2(6)	4.8(2)	0.14(5)	0.060(6)	—	—	—	36.6(1)	99.50
KOM-4s	44.6(6)	11.2(5)	6.1(3)	0.4(1)	0.17(1)	—	—	—	36.8(2)	99.27
KOM-3s	51.0(3)	7.9(2)	6.5(3)	1.1(1)	0.36(1)	—	—	—	34.3(2)	101.16
KOM-10s	43.3(5)	12.1(3)	6.8(3)	2.2(2)	0.24(1)	—	—	—	34.9(2)	99.54
KOM-26s	42.5(7)	13.2(4)	6.6(4)	2.4(3)	0.23(1)	—	—	—	34.9(2)	99.83
KOM-9s	43.1(6)	10.0(2)	9.3(3)	2.6(2)	0.37(3)	—	—	—	34.1(4)	99.47
Ni-Co-W-Doped Experiments										
KOM-16s	13.9(4)	48.5(4)	—	—[3]	—[3]	6.7(1)	—[2]	—	30.1(2)	99.20
KOM-20s	23.5(3)	36.0(5)	—	—[2]	—[2]	8.3(2)	—[2]	—	33.0(3)	100.80
KOM-13	36.6(4)	22.1(4)	—	0.26(3)	0.067(9)	6.6(1)	—[2]	—	34.7(2)	100.33
KOM-11s	48.6(6)	11.7(3)	—	0.7(2)	0.24(1)	4.6(1)	0.06(1)	—	34.7(2)	100.60
Ni-V-Doped Experiments										
KOM-19s	14.0(3)	56.4(3)	—	—[3]	—[3]	—	—	0.014(1)	30.4(3)	100.81
KOM-23s	25.9(8)	41.1(9)	—	—[2]	0.015(6)	—	—	0.013(1)	33.3(4)	100.33
KOM-22s	39.9(7)	24.8(6)	—	0.18(4)	0.060(4)	—	—	0.10(2)	35.9(2)	100.94
KOM-18s	47.5(3)	17.7(3)	—	0.54(6)	0.21(1)	—	—	0.6(2)	34.4(2)	100.95

Notes: Units in parentheses as in Table 2. Abbreviations as in Table 1.
[1]Sulfide melt quenched to a glass.
[2]Concentration is at or below detection limit.
[3]Not determined.

log $D_M^{\text{Sulfide Melt/Silicate Melt}}$ versus log $f_{S_2}^{1/2}$ − log $f_{O_2}^{1/2}$ slopes that are consistent with their probable valence states (3+ and 2+, respectively; Table 8).

The Cr result is especially significant. The behavior of Cr in S-free systems has been investigated in studies of both terrestrial and lunar basalt compositions (Akella et al., 1976; Huebner et al., 1976; Schreiber and Haskin, 1976; Barnes, 1986; Murck and Campbell, 1986; Seifert and Ringwood, 1988; Roeder and Reynolds, 1991; Mikouchi et al., 1994). One of the fundamental observations to come out of these investigations is that the solubility of Cr in spinel-saturated silicate melts varies systematically with temperature, melt composition, and f_{O_2}. Although this effect has been attributed primarily to variations in the Cr^{2+}/Cr^{3+} ratio of the silicate melt with changing conditions, the valence state of Cr as a function of f_{O_2} has only been directly measured in an Fe-free system (Schreiber and Haskin, 1976). Our experimental results are consistent with Cr^{3+} being the dominant species at 1350°C to conditions as reducing as the IQF oxygen buffer.

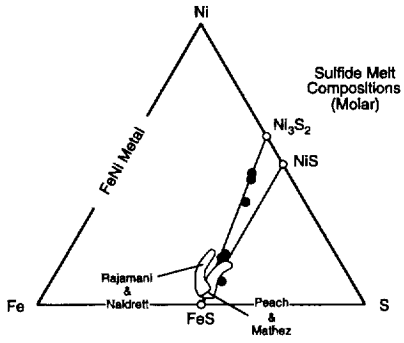

Fig. 4. Ternary plot of Fe-Ni-S system comparing compositions of sulfide melts from Ni partitioning experiments performed on the Fo86 starting composition (filled circles) with those from the experimental studies of Rajamani and Naldrett (1978) and Peach and Mathez (1993). Shown for reference are the FeS-NiS and FeS-Ni_3S_2 joins.

There are at least three lines of evidence that support a low Cr^{2+}/Cr^{3+} ratio in our silicate melts. The first, mentioned above, is that the slope of log $D_{Cr}^{\text{Sulfide Melt/Silicate Melt}}$ versus log $f_{S_2}^{1/2}$ − log $f_{O_2}^{1/2}$ (1.37 ± 0.16) is within 2σ of the value expected for Cr^{3+} (1.50). Although some percentage (~25%) of the total Cr could be present as Cr^{2+}, none is required. For comparison, Schreiber and Haskin (1976) reported 80% of the total Cr in their silicate melts to be divalent in simple system (CaO-MgO-Al_2O_3-SiO_2) experiments performed at 1500–1550°C and f_{O_2} conditions near IQF. The second important observation is that the olivine/silicate melt partition coefficient for Cr measured in our experiments (0.62 ± 0.03) does not vary systematically with decreasing f_{O_2}, as might be expected if the Cr^{2+}/Cr^{3+} ratio were changing. A significant increase in the Cr^{2+}/Cr^{3+} ratio of the silicate melt with decreasing f_{O_2} should result in an increase in the olivine/silicate melt partition coefficient (Schreiber and Haskin, 1976). Mikouchi et al. (1994) also reported a nearly constant olivine/silicate melt partition coefficient for Cr in 1 atm gas-mixing experiments performed at 1225 and 1400°C, with f_{O_2} conditions ranging from 4 log units above to 2 log units below the IW buffer. One caveat to this observation comes from preliminary experiments which

TABLE 8. Regression parameters for logarithm of sulfide melt/silicate melt partition coefficient versus one-half the logarithm of the sulfur fugacity/oxygen fugacity ratio.

$$\log D_i^{\text{Sulfide/Silicate}} = m \frac{1}{2} \log \frac{f_{S_2}}{f_{O_2}} + b$$

Element	Number of Expts.	m	b	r^2	Calculated Valence	Possible Valence
Weight Ratio Partition Coefficients						
V	4	1.36(17)	-5.9(6)	0.9742	2.80+	3+-4+
Cr	10	1.37(8)	-5.3(3)	0.9733	2.74+	2+-3+
Mn	11	1.09(6)	-4.7(2)	0.9737	2.18+	2+
Fe	15	0.68(3)	-1.82(11)	0.9761	1.36+	2+-3+
Co	4	0.69(5)	-0.88(20)	0.9878	1.38+	2+
Ni	13	0.65(4)	0.64(15)	0.9570	1.30+	2+
Cu	7	0.38(3)	1.27(10)	0.9768	0.76+	1+-2+
Molar Ratio Partition Coefficients						
V	4	1.36(16)	-5.6(6)	0.9728	2.80+	3+-4+
Cr	10	1.38(8)	-5.0(3)	0.9753	2.76+	2+-3+
Mn	11	1.09(6)	-4.4(2)	0.9744	2.18+	2+
Fe	15	0.68(3)	-1.50(11)	0.9753	1.36+	2+-3+
Co	4	0.69(6)	-0.55(22)	0.9859	1.38+	2+
Ni	13	0.65(4)	0.97(16)	0.9547	1.30+	2+
Cu	7	0.38(2)	1.59(8)	0.9846	0.76+	1+-2+

Notes: Units in parentheses are 1σ uncertainties on regression parameters.

suggest that the olivine/silicate melt partition coefficient for Cr^{2+} (0.73) may be only moderately larger than that for Cr^{3+} (0.65) in an Fe-free system (Hanson et al., 1996). The third line of evidence for the lack of significant Cr^{2+} in our experiments is that the abundance of Cr in the silicate melt does not vary systematically as a function of f_{O_2}. The experiments that were doped with higher concentrations of Cr have systematically higher Cr in the silicate melt, but the abundance does not increase with decreasing f_{O_2}. A possible explanation for the difference between our results and those from simple-system experiments is that the presence of Fe^{3+} in the silicate melt may shift the Cr^{3+}/Cr^{2+} transition to

TABLE 9. Experimentally-determined sulfide melt/silicate melt partition coefficients.

Experiment	$\log f_{S_2}^{1/2} - \log f_{O_2}^{1/2}$	D_V	D_{Cr}	D_{Mn}	D_{Fe}	D_{Co}	D_{Ni}	D_{Cu}	D_W
Ni-Doped Experiments									
Fo86-8s	2.70	—	—	—	1.88(2)	—	572(7)	—	—
Fo86-5s	2.95	—	—	—	2.43(2)	—	619(5)	—	—
Fo86-9s	3.25	—	—	—	3.29(3)	—	649(15)	—	—
Fo86-15s	3.55	—	—	—	6.63(7)	—	760(30)	—	—
Fo86-14s	3.95	—	—	—	8.25(6)	—	1600(60)	—	—
Fo86-10s	4.40	—	—	—	20.1(4)	—	2160(160)	—	—
Ni-Cr-Cu-Doped Experiments									
KOM-1s	3.05	—	—	—	2.29(6)	—	540(10)	250(20)	—
KOM-6s	3.25	—	0.13(3)	0.06(3)	2.40(6)	—	550(10)	313(9)	—
KOM-15s	3.65	—	0.39(5)	0.26(4)	5.0(6)	—	1100(100)	500(100)	—
KOM-4s	4.10	—	2.2(2)	0.68(2)	8.4(1)	—	1430(50)	690(50)	—
KOM-3s	4.40	—	7.2(3)	1.49(4)	17.6(3)	—	—	960(50)	—
KOM-10s	4.40	—	4.8(2)	1.07(5)	13.3(3)	—	3600(200)	900(100)	—
KOM-26s[1]	4.40	—	4.9(2)	0.99(5)	13.4(5)	—	2400(300)	690(70)	—
KOM-9s	4.55	—	6.8(3)	1.8(1)	18.9(5)	—	—	970(50)	—
Ni-Co-W-Doped Experiments									
KOM-16s	3.05	—	—	—	1.53(4)	17.7(5)	510(11)	—	—
KOM-20s	3.25	—	—	—	2.72(6)	24.3(9)	580(30)	—	—
KOM-13s	3.95	—	1.8(1)	0.30(2)	5.7(2)	62(4)	1600(100)	—	—
KOM-11s	4.40		6.3(5)	1.09(3)	16.9(4)	164(7)	4400(400)	—	0.113(8)
Ni-V-Doped Experiments									
KOM-19s	3.05	0.025(1)	—	—	1.58(11)	—	410(20)	—	—
KOM-23s	3.25	0.022(1)	—	0.07(1)	2.80(7)	—	550(20)	—	—
KOM-22s	3.80	0.18(1)	1.1(1)	0.26(1)	5.2(2)	—	1170(80)	—	—
KOM-18s	4.40	1.3(1)	4.9(2)	0.94(4)	15.8(7)	—	3800(400)	—	—

Notes: Units in parentheses represent 1 σ uncertainties of the least units cited calculated by propagating the standard deviation of the mean.
[1]Reversal experiment.

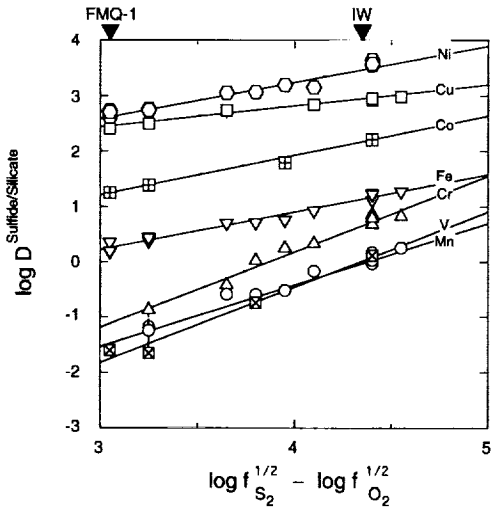

Fig. 5. Plot of log $D^{\text{Sulfide Melt/Silicate Melt}}$ versus log $f_{S_2}^{1/2}$ − log $f_{O_2}^{1/2}$ illustrating the dependence of the sulfide melt/silicate melt partitioning of Ni (hexagons), Cu (squares), Co (squares with plusses), Fe (upside-down triangles), Cr (triangles), Mn (circles), and V (squares with crosses) on f_{O_2} and f_{S_2} conditions. Error bars are 1σ. Where error bars are not shown, they are smaller than symbols.

more reducing conditions, as suggested by Schreiber and Haskin (1976). It is also possible that the presence of S^{2-} dissolved in the silicate melt affects Cr oxidation-reduction equilibria.

The slopes of the log $D_M^{\text{Sulfide Melt/Silicate Melt}}$ versus log $f_{S_2}^{1/2}$ − log $f_{O_2}^{1/2}$ regression lines for Fe (0.68 ± 0.03 vs. 1.0), Co (0.69 ± 0.05 vs. 1.0), Ni (0.65 ± 0.04 vs. 1.0), and Cu (0.38 ± 0.03 vs. 0.5) are shallower than expected in Fig. 5, demonstrating that the f_{O_2}/f_{S_2} dependencies of their sulfide melt/silicate melt partition coefficients are weaker than would be predicted on the basis of their valence states. Peach and Mathez (1993) also noted weaker than expected f_{O_2}/f_{S_2} dependencies for the partitioning of Fe (0.78) and Ni (0.60) between sulfide melt and silicate melt in experiments performed at 8 kbar, 1450°C. If these slopes resulted solely from the relationship given by Eqn. 5, it would require that a significant percentage of each element be dissolved in the silicate melt as a neutral species even at f_{O_2} conditions 1 log unit below the FMQ buffer. This is highly improbable, especially given the constancy of the olivine/silicate melt partition coefficients for these elements over the range of f_{O_2} conditions investigated. A second possibility is that the ratio of the activity coefficients for these elements in sulfide and silicate melts ($\gamma_M^{\text{Silicate}}/\gamma_M^{\text{Sulfide}}$) is variable due to the variation in the major element compositions of the coexisting liquids. This should lead to curvature in the log $D_M^{\text{Sulfide Melt/Silicate Melt}}$ vs. log $f_{S_2}^{1/2}$ − log $f_{O_2}^{1/2}$ relationship, however, and none is evident.

Another mechanism for producing weaker than expected f_{O_2}/f_{S_2} dependencies is for some percentage of the Fe, Co, Ni, and Cu to be bonded with S^{2-}, rather than O^{2-}, anions in the silicate melt, as suggested for Ni by Peach and Mathez (1993). At conditions more reducing than FMQ, S dissolves in silicate melts as S^{2-} anions by displacing O^{2-} anions that are bonded with metal cations such as Fe^{2+} (Fincham and Richardson, 1954; Haughton et al., 1974). This solubility mechanism should leave some percentage of the strongly

TABLE 10. Experimentally-determined olivine/silicate melt partition coefficients.

Experiment	$\log f_{S_2}^{1/2} - \log f_{O_2}^{1/2}$	D_V	D_{Cr}	D_{Mn}	D_{Fe}	D_{Co}	D_{Ni}	D_{Cu}	D_W
Ni-Doped Experiments									
Fo86-8s	2.70	—	—	—	1.07(1)	—	7.46(19)	—	—
Fo86-5s	2.95	—	—	—	1.20(1)	—	7.24(7)	—	—
Fo86-9s	3.25	—	—	—	1.13(1)	—	6.48(16)	—	—
Fo86-15s	3.55	—	—	—	1.09(1)	—	7.0(3)	—	—
Fo86-14s	3.95	—	—	—	1.16(1)	—	7.1(3)	—	—
Fo86-10s	4.40	—	—	—	1.14(2)	—	4.0(3)	—	—
Ni-Cr-Cu-Doped Experiments									
KOM-1s	3.05	—	0.642(4)	0.847(4)	0.972(2)	—	6.74(6)	0.096(9)	—
KOM-6s	3.25	—	0.593(8)	0.760(3)	0.866(5)	—	5.74(4)	0.075(8)	—
KOM-15s	3.65	—	0.611(3)	0.713(4)	0.898(5)	—	5.6(1)	0.133(7)	—
KOM-4s	4.10	—	0.657(6)	0.714(4)	0.897(16)	—	6.2(2)	0.11(2)	—
KOM-3s	4.40	—	0.631(2)	0.707(3)	0.954(7)	—	—	0.19(3)	—
KOM-10s	4.40	—	0.64(1)	0.692(3)	0.907(8)	—	7.0(7)	0.09(1)	—
KOM-26s[1]	4.40	—	0.640(2)	0.681(2)	0.864(7)	—	6.4(6)	—	—
KOM-9s	4.55	—	0.631(2)	0.681(3)	0.905(9)	—	—	0.08(1)	—
Ni-Co-W-Doped Experiments									
KOM-16s	3.05	—	0.58(1)	0.69(1)	0.957(7)	1.81(6)	5.5(2)	—	0.016(1)
KOM-20s	3.25	—	0.594(3)	0.731(5)	0.872(4)	1.954(4)	5.7(1)	—	0.053(2)
KOM-13s	3.95	—	0.629(6)	0.717(5)	0.927(7)	1.93(2)	5.4(2)	—	0.039(2)
KOM-11s	4.40	—	0.656(4)	0.702(3)	0.916(10)	1.96(2)	7.1(6)	—	0.054(3)
Ni-V-Doped Experiments									
KOM-19s	3.05	0.096(1)	0.617(4)	0.736(3)	0.877(7)	—	5.97(6)	—	—
KOM-23s	3.25	0.099(1)	0.580(3)	0.741(3)	0.857(5)	—	5.47(8)	—	—
KOM-22s	3.80	0.159(1)	0.595(5)	0.713(5)	0.899(7)	—	5.6(3)	—	—
KOM-18s	4.40	0.340(1)	0.648(4)	0.707(2)	0.879(10)	—	4.5(3)	—	—

Notes: Units in parentheses represent 1σ uncertainties calculated by propagating the standard deviation of the mean.
[1]Reversal experiment.

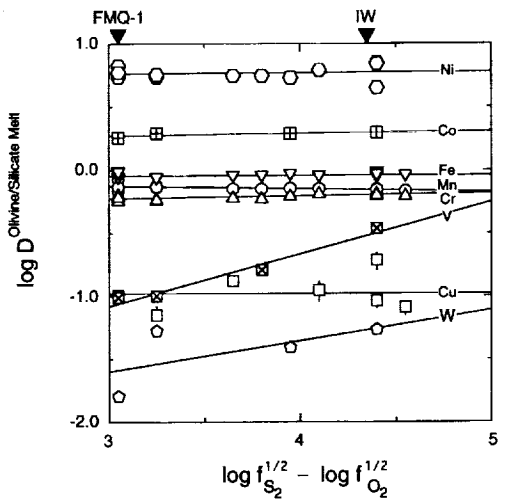

Fig. 6. Plot of log $D^{\text{Olivine/Silicate Melt}}$ versus log $f_{S_2}^{1/2}$ − log $f_{O_2}^{1/2}$ illustrating the constancy of the olivine/silicate melt partition coefficients for of Ni (hexagons), Co (squares with plusses), Fe (upside-down triangles), Mn (circles), Cr (triangles), and Cu (squares) with changing f_{O_2} and f_{S_2} conditions. The systematic increase in the olivine/silicate melt partition coefficient for V (squares with crosses), and possibly W, (pentagons) is attributable to changing valence state with decreasing f_{O_2}. Error bars are 1σ. Where error bars are not shown, they are smaller than symbols.

chalcophile elements to bond with S^{2-} rather than O^{2-} anions in the silicate melt. If the sulfide melt/silicate melt exchange reaction given in Eqn. 1 is modified to take this into account, the governing reaction becomes:

$$M_X O_Y S_{Z_1}^{\text{Silicate Melt}} + \frac{Z_2}{2} S_2^{\text{Gas}} = M_X S_{Z_2}^{\text{Sulfide Melt}} + \frac{Y}{2} O_2^{\text{Gas}} + \frac{Z_1}{2} S_2^{\text{Gas}} \quad (6)$$

where $Y + Z_1 = X$ for divalent cations. Following steps similar to Eqns. 2 through 4, the expression relating $D_M^{\text{Sulfide Melt/Silicate Melt}}$ to f_{O_2} and f_{S_2} becomes:

$$\log D_M^{\text{Sulfide Melt/Silicate Melt}} = \frac{1}{2X}\left[(Z_2 - Z_1)\log f_{S_2} - Y \log f_{O_2}\right] + C \quad (7)$$

Different values of Z_1 can be substituted into this expression to account for various percentages of MS dissolved in the silicate melt. Experimentally determined log $D_M^{\text{Sulfide Melt/Silicate Melt}}$ values can then be regressed against $(Z_2 - Z_1)\log f_{S_2} - Y \log f_{O_2}$ and the slope compared with a theoretical value. If, for example, Ni is dissolved in the sulfide melt as Ni_3S_2 (Fig. 4) and the Ni^{2+} dissolved in the silicate melt is a mixture of NiO and NiS, then substituting the correct value for Z_1 into Eqn. 7 will result in a log $D_{Ni}^{\text{Sulfide Melt/Silicate Melt}}$ vs. $(Z_2 - Z_1)\log f_{S_2} - Y \log f_{O_2}$ regression line with a slope of 0.17.

This approach was used to estimate that ~31% of the total Ni in the silicate melt must be bonded to S^{2-} anions in order to explain our $D_{Ni}^{\text{Sulfide Melt/Silicate Melt}}$ values. A similar treatment of the sulfide melt/silicate melt partition coefficients for Ni determined experimentally by Peach and Mathez (1993) results in ~16% of the total Ni in their silicate melts being present as NiS. Calculations for the Cu and Co data, assuming that all Cu is monovalent and all Co is divalent in both liquids, indicates that ~20% of the total Cu in the silicate melt must be Cu_2S, and that ~31% of the Co must be CoS.

Although these percentages are consistent with the concentration of S dissolved in the silicate melts, there are two observations that argue against this mechanism for producing the observed f_{O_2}/f_{S_2} dependencies. The first is that the presence of sulfide species in the silicate melt at the concentrations required to explain our data should produce a noticeable decrease in olivine/silicate melt partition coefficients, and none is observed. The second is that the low concentration of S in the silicate melts precludes this mechanism as an explanation for the behavior of Fe. That the log $D_M^{\text{Sulfide Melt/Silicate Melt}}$ vs. log $f_{S_2}^{1/2}$ − log $f_{O_2}^{1/2}$ slopes for Fe, Co, and Ni are within uncertainty of each other suggests that a single mechanism may be responsible for all three. Capobianco and Amelin (1994) determined metal/silicate melt partition coefficients for Ni and Co in the CaO-MgO-Al_2O_3-SiO_2 system over a range of temperature and f_{O_2} conditions. Their experimental results show an f_{O_2} dependence for partitioning at 1300–1425°C that is most readily explained by f_{O_2}-induced changes in silicate melt structure. It is possible that the low f_{O_2}/f_{S_2} dependencies for Fe, Co, Ni, and Cu found in our experiments are related to similar melt structural changes.

A comparison of the f_{O_2}/f_{S_2} dependencies of the sulfide melt/silicate melt (Fig. 5) and of the olivine/silicate melt (Fig. 6) partitioning of V demonstrates that its behavior is more complicated than the other elements studied. The strong, linear increase in log $D_V^{\text{Olivine/Silicate Melt}}$ with decreasing f_{O_2}/f_{S_2} ratio (Fig. 6) indicates that V is undergoing a change in valence state related to changing f_{O_2}, most likely from 4+ to 3+. This should produce a change in slope in the V partitioning data shown in Fig. 5 (cf. Holzheid et al., 1994; Borisov and Palme, 1995), but none is apparent. It is

TABLE 11. Forsterite contents and Fe/Mg exchange K_D values for San Carlos olivine crucibles and experimentally-produced olivines.

Experiment	Crucibles Fo	K_D	Olivines Fo	K_D
KOM-1s	88.7	0.31	88.7	0.31
KOM-6s	89.9	0.31	90.0	0.31
KOM-15s	91.2	0.32	91.3	0.32
KOM-4s	93.9	0.31	93.9	0.31
KOM-3s	96.2	0.35	96.5	0.32
KOM-10s	96.0	0.33	96.2	0.31
KOM-26s	96.2	0.31	96.3	0.31
KOM-9s	97.4	0.31	97.5	0.30
KOM-16s	88.2	0.33	88.0	0.33
KOM-20s	89.9	0.30	90.0	0.30
KOM-13s	92.3	0.32	92.3	0.32
KOM-11s	96.5	0.33	96.6	0.32
KOM-19s	89.2	0.31	89.5	0.31
KOM-23s	89.6	0.30	89.5	0.30
KOM-22s	91.1	0.31	91.0	0.32
KOM-18s	96.5	0.31	96.6	0.30

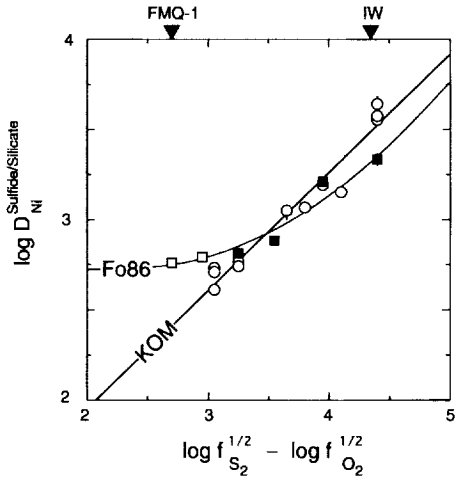

Fig. 7. Plot of log $D_{Ni}^{Sulfide\ Melt/Silicate\ Melt}$ versus log $f_{S_2}^{1/2}$ − log $f_{O_2}^{1/2}$ comparing the linear relationship found in the KOM experiments (open circles) with the curvature found in the experiments performed on the Fo86 starting composition (squares). The Fo86 experiments represented by open squares are olivine saturated, while those represented as filled squares are saturated with an olivine + protoenstatite assemblage. Error bars are 1σ. Where error bars are not shown, they are smaller than symbols.

probable that additional experiments are needed to better define the nature of the relationship between log $D_V^{Sulfide\ Melt/Silicate\ Melt}$ and log $f_{S_2}^{1/2}$ − log $f_{O_2}^{1/2}$.

The systematics of sulfide melt/silicate melt partitioning for Ni determined in the experiments performed on the Fo86 composition differ from those found in the KOM experiments. Figure 7 shows that whereas the Ni data from the komatiite experiments define a linear relationship between log $D_{Ni}^{Sulfide\ Melt/Silicate\ Melt}$ and log $f_{S_2}^{1/2}$ − log $f_{O_2}^{1/2}$, there is curvature in the trend defined by the Fo86 experiments. The sulfide melt/silicate melt partition coefficients from the Fo86 experiments are larger than those from the KOM experiments at high f_{O_2}/f_{S_2} ratio conditions, and comparable or smaller at lower f_{O_2}/f_{S_2} ratios. The simplest explanation for this is a variation in the ratio of the activity coefficients for Ni in silicate and sulfide melts ($\gamma_{Ni}^{Silicate}/\gamma_{Ni}^{Sulfide}$) with changing f_{O_2}/f_{S_2} conditions. Given that temperature and pressure are constant in these experiments, the variation in the activity coefficient ratio must be attributable to the compositional changes occurring in one or both of the coexisting liquids.

The high concentrations of Ni in the sulfide melts (11.2 to 58.6 wt%) could lead to a non-Henrian activity-composition relationship, but the V-doped komatiite experiments have a similar range in Ni (17.7 wt% to 56.4 wt%) and do not show the same partitioning behavior. Therefore, it is probable that the curvature in the Fo86 data is related to the compositional changes occurring in the silicate melt. The most significant variation in the silicate melt composition is a decrease in the concentration of FeO (from 9.1 to 3.68 wt%) with decreasing f_{O_2}/f_{S_2} ratio. Although an even larger variation occurs in the FeO contents of the silicate melts from the KOM experiments (11.9 to 2.94 wt% FeO), there is an important difference between the two sets of experiments. The Fo86 experiments performed at high f_{O_2}/f_{S_2} ratio conditions are saturated with olivine, while the low f_{O_2}/f_{S_2} ratio experiments are saturated with coexisting olivine and low-Ca pyroxene. This demonstrates that as the FeO content of the silicate melt decreases the activity of SiO_2 increases until pyroxene saturation is reached.

Variations in the sulfide capacity (C_s) of the silicate melt (C_s = [wt% S dissolved in the silicate melt] × [$f_{O_2}^{1/2}/f_{S_2}^{1/2}$]) can provide information on whether the compositional changes in the Fo86 silicate melts are significant enough to produce the curvature in Fig. 7. Sulfide capacity is a strong function of the activity of the metal cations that bond with S^{2-} in the silicate melt, especially Fe^{2+} (Fincham and Richardson, 1954; Haughton et al., 1974), and should indicate how the activity of Ni varies in the silicate melt. In binary systems C_s also decreases with increasing SiO_2 activity, as O^{2-} anions bonded solely to metal cations are replaced by O^{2-} anions in tetrahedral coordination with Si^{4+} (Fincham and Richardson, 1954; Abraham et al., 1960; Abraham and Richardson, 1960). Figure 8 shows log C_s vs. FeO content of the silicate melt in our experiments, a relationship that should be linear. The curvature in the Fo86 data (squares) that is apparent in Fig. 8 is independent of any compositional changes occurring in the sulfide melt and is, therefore, indicative of significant changes in the activities of transition metal cations and/or SiO_2 in the silicate melt with decreasing f_{O_2}/f_{S_2} ratio.

Although a decrease in C_s with increasing SiO_2 activity is consistent with other experimental studies, the decrease in $D_{Ni}^{Sulfide\ Melt/Silicate\ Melt}$ is contrary to what would be expected on the basis of the partitioning of Ni between olivine and silicate melt (e.g., Hart and Davis, 1978; Kinzler et al., 1990). There is an inverse relationship between MgO content of the melt and $D_{Ni}^{Olivine/Silicate\ Melt}$ but silicate melts with different SiO_2 and the same MgO content do not show a significant variations in $D_{Ni}^{Olivine/Silicate\ Melt}$. The filled squares

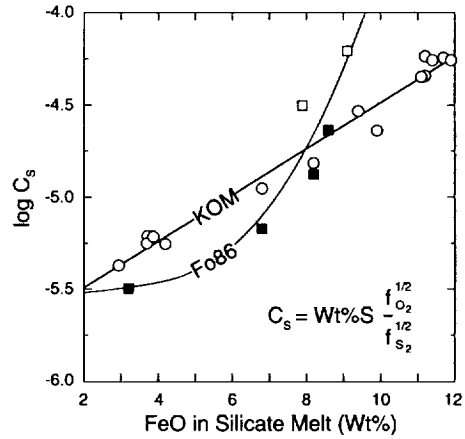

Fig. 8. Plot of the logarithm of the sulfide capacity of the silicate melt (log C_S) versus FeO content comparing the linear relationship found in the KOM experiments (open circles) with the curvature found in the experiments performed on the Fo86 starting composition (squares). The Fo86 experiments represented by open squares are olivine saturated, while those represented as filled squares are saturated with an olivine + protoenstatite assemblage. 1σ error bars are smaller than symbols.

in Figs. 7 and 8 represent Fo86 experiments in which the silicate melt is saturated with coexisting olivine and protoenstatite. The activity of SiO_2 in these experiments is buffered by the coexisting crystalline phases. The relationship between log C_s and FeO for this subset of experiments is nonlinear, indicating that the activity of transition metals in the silicate melt varies substantially even though the activity of SiO_2 does not. Therefore, the variation in Ni activity must be related to some other compositional variable. One important difference between the Fo86 and KOM silicate melts is that the former have unusually low CaO relative to naturally occurring basaltic or ultramafic silicate melts, causing some of the MgO to form $MgAl_2O_4$ complexes in order to stabilize Al in the aluminosilicate network (e.g., Bottinga and Weill, 1972). A spectroscopic study of aluminosilicate glasses along the SiO_2-$MgAl_2O_4$ join found Al in fivefold and sixfold coordination with oxygen rather than the tetrahedral coordination that characterizes alkali aluminosilicate glasses (McMillan and Kirkpatrick, 1992), suggesting that the presence of $MgAl_2O_4$ complexes may influence silicate melt structure. Good linear correlations exist between the calculated mole fraction of $MgAl_2O_4$ in the silicate melt and log $D_{Ni}^{\text{Sulfide Melt/Silicate Melt}}$ (r^2 = 0.9047), and between the molar FeO/$MgAl_2O_4$ ratio of the silicate melt and log C_s (r^2 = 0.9123) for the Fo86 experiments. Although correlation does not demonstrate cause, it is suggestive that the presence of a $MgAl_2O_4$ component in the silicate melt may influence the activity of Ni. These results demonstrate that, in certain cases, experiments performed in simplified analog systems may predict more complicated partitioning behavior than is found in natural systems.

4.2. Modeling Core Formation

In the following sections, core formation in the Earth and in the parent body of Shergottite meteorites (Mars) is modeled as a single-stage equilibrium segregation of metallic phases from mantle silicates using the approach developed by Rammensee and Wänke (1977) as modified by Newsom (1985). Our experimentally determined sulfide melt/silicate melt and olivine/silicate melt partition coefficients are combined with the experimentally determined metal/silicate melt partition coefficients of Schmidt et al. (1989) and of Drake et al. (1989) to evaluate whether the siderophile element abundance pattern in the mantle of either planet is consistent with the equilibrium segregation of sulfide melt ± metal from an olivine-rich mantle at low pressures and temperatures. To account for the differences in experimental temperatures among this study (1350°C) and that of Schmidt et al. (1989; 1300°C) and of Drake et al. (1989; 1260°C) partition coefficients were calculated relative to the IW oxygen buffer using linear equations such as those given in Table 8. No other form of temperature correction was applied to the partition coefficients. Although phase composition will undoubtedly affect partitioning (e.g., Hillgren et al., 1996), our experimental results indicate that for natural mafic and ultramafic silicate melts compositional effects will be minor compared to variations related to f_{O_2}/f_{S_2} conditions.

The bulk (sulfide + metal)/total-silicate partition coefficient ($D^{m/s}$) is given by:

$$D^{m/s} = \frac{D_i}{F_{liq} + (C^{sol}/C^{liq})(1 - F_{liq})} \quad (8)$$

where D_i is the (sulfide + metal)/silicate melt partition coefficient for a given siderophile element, F_{liq} is the fraction of silicate melt divided by the total fraction of silicates, and C^{sol}/C^{liq} is the silicate solid/silicate melt partition coefficient for a given siderophile element. This expression is substituted into the equation:

$$X = \frac{a - 1}{D^{m/s} + a - 1} \quad (9)$$

where X is the weight fraction of sulfide segregated from the mantle to form the core, and a is the depletion factor for a given element. A depletion factor is the ratio of the concentrations of a siderophile element (C_i) to a refractory lithophile element (C_j) in C1 chondrites divided by the same ratio in the silicate portion of a planet ($a = [C_i/C_j]_{C1}/[C_i/C_j]_{Mantle+Crust}$). Equation 9 predicts the mass of the core that is required to produce the observed siderophile element/lithophile element fractionation as a function of the extent of silicate partial melting that accompanied core formation. Performing this calculation for a series of siderophile elements using known depletion factors and experimentally determined partition coefficients produces a series of curves relating core size to extent of silicate partial melting. If the abundances of the siderophile elements in the mantle of a planet can be explained by a core-forming process for which the given partition coefficients are appropriate, all of the curves will intersect at a point coinciding with the mass of the core of the planet, and with the extent of silicate partial melting that accompanied core segregation.

4.3. The Role of Sulfide in Core Formation in the Earth

The origin of the siderophile element abundance pattern in the upper mantle of the Earth is a long-standing problem in geochemistry. Ringwood (1966) first noted that the absolute and relative abundances of the siderophile elements cannot be explained by the equilibrium segregation of metal from silicate on the basis of known metal/silicate partition coefficients. Four models have subsequently been proposed to explain the pattern: (1) heterogeneous accretion, in which a veneer of chondritic material is accreted following segregation of the core and mixed into the upper mantle (Morgan et al., 1980; Wänke, 1981); (2) inefficient core formation, in which some percentage of metal remains in the mantle following segregation of the core, and is subsequently oxidized (Jones and Drake, 1986); (3) equilibrium segregation of a sulfide melt from the upper mantle (Brett, 1984); and (4) segregation of core-forming material from a magma ocean under extreme pressure or temperature conditions (Murthy, 1991; Walker et al., 1993; Li and Agee, 1996).

The equilibrium sulfide segregation model was conceived on the basis of the observations that the density of the outer core is 10% lower than that of a pure FeNi alloy at comparable conditions, requiring the presence of a light alloying element or elements (Birch, 1961, 1964), and that sulfide melt/silicate melt partition coefficients for siderophile ele-

TABLE 12. Parameters used in core segregation modeling.

Depletion Factors							Partition Coefficients						
V	Cr	Mn	Fe	Co	Ni	Cu	V	Cr	Mn	Fe	Co	Ni	Cu
Earth							*Metal/Silicate Melt*						
2.0	2.3	5.3	—	12.8	14.0	12.1	0.007	0.12	0.004	—	71	1200	13
							Sulfide Melt/Silicate Melt						
							0.02	0.08	0.03	—	17	420	290
							Olivine/Silicate Melt						
							0.34	0.61	0.71	—	1.9	5.9	0.11
Shergittite Parent Body							*Metal/Silicate Melt*						
—	1.0	1.0	2.18	14.9	55.7	46.4	—	0.154	0.0055	3.35	93	1565	20
							Sulfide Melt/Silicate Melt						
							—	4.96	1.09	14.07	140	3171	864
							Olivine/Silicate Melt						
							—	0.61	0.71	0.90	1.9	5.9	0.11
							Low-Ca pyroxene/Silicate Melt						
							—	—	—	0.59	—	—	—
							High-Ca pyroxene/Silicate Melt						
							—	—	—	0.25	—	—	—

ments tend to be smaller than metal/silicate melt partition coefficients at comparable conditions (Brett, 1984). Brett (1984) proposed that core formation took place through the segregation of sulfide melt (23 wt% S; 8 wt% O) from a solid mantle. According to this model the siderophile element abundance pattern of the mantle was established by equilibrium partitioning between silicate minerals and sulfide melt at low pressures and temperatures, as the melt migrated through the shallow mantle via porous flow. At greater depth, the melts aggregated to form larger, faster-moving bodies that did not maintain chemical equilibrium with the surrounding mantle. The S content of the melt decreased through an unspecified reaction in the deep mantle before the melt was added to the core.

Brett (1984) used partition coefficients from several different low-pressure experimental studies to test the equilibrium sulfide segregation model against upper mantle siderophile element abundances. These partition coefficients were determined from experiments in which the f_{O_2}/f_{S_2} conditions were not controlled. Here we revisit the model of Brett (1984) and test it using f_{O_2}/f_{S_2}-sensitive partition coefficients. The depletion factors used in our modeling were calculated using the primitive mantle abundances of Jagoutz et al. (1979) and the C1 abundances of Anders and Grevesse (1989), and are normalized to the refractory lithophile element La (Table 12). Brett (1984) proposed that upper mantle conditions during core formation were an f_{S_2} equivalent to the FeFeS sulfur buffer (log $f_{S_2} = -4.10$ at 1350°C), and an f_{O_2} value equivalent to the IW oxygen buffer (log $f_{O_2} = -10.20$ at 1350°C). These conditions correspond to a log $f_{S_2}^{1/2}$ − log $f_{O_2}^{1/2}$ value of 3.05.

The results from our modeling are presented in Fig. 9. Because of the incompatible behavior of V, Cr, and Mn with respect to sulfide melt at these conditions, their observed fractionation from La in the upper mantle of the Earth could only be produced by formation of an unreasonably large core (91% to 99% of the Earth's mass). This does not invalidate the sulfide model, however, because it has been argued that the depletion pattern for these elements is related to their relative volatilities and, therefore, was established by accretionary processes rather than core formation (Drake et al., 1989). The sulfide model is fairly successful for explaining the Co abundance of the mantle requiring a core that comprises 41 wt% of the Earth and an extent of silicate partial melting of 100% accompanying core formation. The crossover point for Ni and Cu at these conditions, however, only allows for a core that is 3.6% of the mass of the Earth, with core formation accompanied by 96% silicate partial melting. This core is too small by an order of magnitude. The lack of agreement among Ni, Co, and Cu precludes equilibrium segregation of a sulfide melt at low temperatures and pressures as the appropriate model to explain the siderophile element abundance pattern of the mantle of the Earth. Choos-

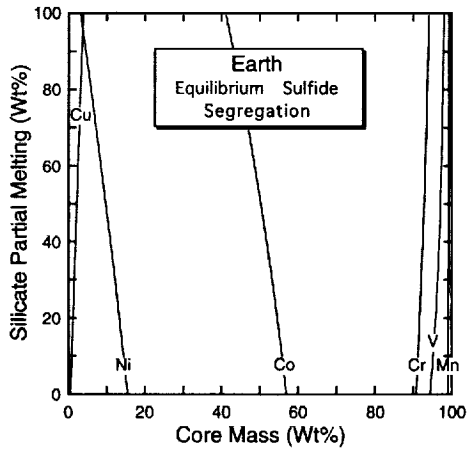

Fig. 9. Plot of core mass versus extent of silicate partial melting that accompanied core segregation showing the results of equilibrium sulfide segregation modeling for V, Cr, Mn, Co, Ni, and Cu depletions in the upper mantle of the Earth. Core formation f_{O_2}/f_{S_2} conditions tested in this model are log $f_{O_2} = -10.2$ and log $f_{S_2} = -4.1$ at 1350°C.

ing f_{O_2}/f_{S_2} conditions other than those suggested by Brett (1984) does not improve the modeling result, because the f_{O_2}/f_{S_2} dependence of log $D_{Ni}^{Sulfide\ Melt/Silicate\ Melt}$ and log $D_{Co}^{Sulfide\ Melt/Silicate\ Melt}$ are nearly identical (Table 8). Equilibration of a core-forming sulfide melt with mantle silicates at low pressures and temperatures cannot explain the mantle's nearly chondritic Ni/Co ratio at any reasonable set of f_{O_2}/f_{S_2} conditions.

An alternative to segregation of a single sulfide phase to form the core is segregation of a mixture of sulfide melt and metal, accompanied by partial melting of the silicate mantle (Jones and Drake, 1986; Newsom, 1990). This process would also have occurred at low temperatures. We tested a model of segregation of a mixture consisting of 27 wt% sulfide melt (containing 35 wt% S) and 73 wt% metal. This combination will produce an outer core with a S content of 10 wt%, in agreement with current geophysical estimates (e.g., Poirier, 1994). The results from this type of model are similar to those for extraction of sulfide alone. A large core (88% to 100% of the mass of the Earth) is required to explain the abundances of V, Cr, and Mn, while a very small core (5.2% of the Earth mass) is needed to explain Ni and Cu. Once again the abundance of Co in the upper mantle of the Earth can be reasonably accounted for (a 29 wt% core), assuming no partial melting of the silicate. This result agrees with similar calculations performed by Jones and Drake (1986) and by Newsom (1990). Both of these studies concluded that some percentage of the segregating material must be trapped in the mantle in order for this type of core formation to be consistent with known siderophile element abundances.

Our experimentally determined partition coefficients are not appropriate for testing the possibility that sulfide melt segregated from a molten upper mantle at extreme pressure-temperature conditions to form the core. Experimental studies demonstrate that sulfide melt/silicate melt partition coefficients for some moderately siderophile elements decrease with increasing temperature (Walker et al., 1993) and pressure (Li and Agee, 1996). Further, the experimental results of Li and Agee (1996) suggest a convergence of the partition coefficients for Ni and Co with increasing pressure. Although these experimental studies indicate that equilibrium sulfide melt/silicate melt partitioning may have played a role in forming the core of the Earth, neither provides a completely satisfactory resolution to the siderophile element overabundance problem. The experimentally determined partition coefficients of Walker et al. (1993) predict mantle Ge/Ni and P/Ni ratios that are too high, and the silicate (34.6 wt% SiO_2; 48.0 wt% MgO) and sulfide (29.7 wt% S) melts produced in the experiments of Li and Agee (1996) are poor analogs for the mantle (45.2 wt% SiO_2; 38.3 wt% MgO) and core ($\leq$12 wt% S), of the Earth, respectively.

4.4. Size and Composition of the Martian Core

The Shergottites-Nahklites-Chassigny (SNC) meteorites are a group of basaltic achondrites whose major and trace element compositions (Stolper, 1979; Stolper and McSween, 1979) and young crystallization ages (McSween et al., 1979; Walker et al., 1979) indicate that their parent body was one of the terrestrial planets rather than an asteroid. A comparison of Viking measurements of the Martian atmosphere with the noble gases trapped in Shergottite impact melt glasses provides the strongest evidence that the Shergottite parent body (SPB) is Mars (Bogard and Johnson, 1983). The abundances of siderophile elements in these meteorites, therefore, provide clues to the processes involved in the formation of the Martian core.

The size and composition of the Martian core is poorly constrained by geophysical measurements due to the large uncertainties associated with the planet's moment of inertia (Bills, 1996). Alternative approaches to determining the size and composition of the Martian core can be broadly divided into cosmochemical and geochemical models. Cosmochemical estimates rely on determinations of the mean density of Mars (Bills and Ferrari, 1978), theoretical calculations of the temperatures at which equilibrium solids condense from a gas of solar composition (Grossman, 1972; Lewis, 1972), compositional data from the Viking and Mars 5 missions (Owen et al., 1977; Surkov, 1977), and the compositions of various classes of chondritic meteorites. Geochemical approaches are based, at least in part, on chemical analyses of SNC meteorites.

The least complicated of the cosmochemical approaches assumes that condensation of equilibrium solids from a gas of solar composition took place in a nebula with an adiabatic pressure-temperature gradient. Mars is assumed to have accreted from a restricted annular zone with a lower mean temperature than that from which the Earth accreted (Goettel, 1983). This model predicts a relatively massive core (26.4% of the mass of Mars) that is moderately rich in S (17.6 wt%) (Table 13). A modified equilibrium condensation model in which feeding zones overlap predicts a similar core mass (25.7%) and a higher S content (33.8 wt%; Weidenschilling, 1976). The high-S core compositions predicted by these models result from the assumption that Mars accreted from material in a lower temperature portion of the nebula and, thus, contains a higher proportion of volatile elements and oxidized Fe than the Earth. A second class of cosmochemical model uses mixtures of chondritic meteorites to produce a bulk composition that is consistent with the existing data on Mars (Anderson, 1972; Anders and Owen, 1977; Morgan and Anders, 1979; Ringwood, 1981). All metal and S is then partitioned into the core. These models predict a range of core masses (11.9 to 19.0 wt%) and S contents (3.5 to 18.6 wt%) (Table 13), depending the assumptions that go into the model and the data used to constrain it.

Two groups have used the geochemical approach to estimate the size and composition of the Martian core. They derived similar estimates for the siderophile element abundance pattern of the SPB mantle on the basis of SNC meteorite compositions. Both groups concluded that the SPB mantle is characterized by a Co/Ni ratio that is ~5–10 times chondritic, and pronounced depletions in elements with chalcophile affinities. They used these compositional characteristics to support the existence of a high-S core. Wänke and Dreibus (1988) assumed that Mars contains Fe and Ni in chondritic proportions relative to Si and estimated a S abundance on the basis of their heterogeneous accretion model.

TABLE 13. Comparison of model Martian core compositions.

	1	2	3	4	5	6	7
Mantle + crust							
Mg/(Mg+Fe)	0.79	0.77	0.67	0.77	0.66	0.75	0.72
Relative Mass	73.6	74.3	88.1	81.0	81.8	78.3	80.8
Core							
Fe	76.2	60.4	72.0	88.1	63.7	77.8	88.1
Ni	6.2	5.8	9.3	8.0	8.2	8.0	11.1
Co	—	—	—	0.4	—	—	0.3
Cu	—	—	—	—	—	—	0.1
S	17.6	33.8	18.6	3.5	9.3	14.2	0.4
O	—	—	—	—	18.7	—	—
Relative Mass	26.4	25.7	11.9	19.0	18.2	21.7	19.2

1: Equilibrium condensation from nebula of solar composition assuming adiabatic pressure-temperature gradient (Goettel, 1983);
2: Equilibrium condensation with modified accretion zones (Weidenschilling, 1972);
3: Mixture of chondritic meteorites constrained by mean density and moment of inertia (Anderson, 1972);
4: Seven-component chondrite mixture constrained by Viking and Mars 5 isotopic and compositional data (Morgan and Anders, 1979);
5: 30% Orgueil CI chondrite + 70% high temperature component mixture (Ringwood, 1981);
6: Fe mass balance constrained by SNC estimate of mantle FeO content (Wänke and Dreibus, 1988);
7: This study.

The compositions of SNC meteorites were used to determine the FeO content of the Martian mantle, and the Fe in their bulk composition was mass balanced between the SPB mantle and core. They partitioned all Ni and S into the core. Their model predicts a core mass of 21.7% and a S content of 14.2 wt% (Table 13). Treiman et al. (1986) used analyses of SNC meteorites to estimate the geochemical characteristics of the SPB mantle and discussed the broad constraints placed on core formation by the relative abundances of Ni and Co. Treiman et al. (1987) modeled the SPB mantle abundances of Ni, Co, W, P, and Mo to constrain core formation. They used a model in which siderophile elements were partitioned among four phases (solid metal, liquid metal, solid silicate, liquid silicate) without normalizing their concentrations to that of a refractory lithophile element. Treiman et al. (1987) estimated that the ambient f_{O_2} conditions during SPB core formation were 1 log unit below the IW buffer, and predicted a large core (25 to 35 wt%) composed of a 50:50 mixture of metal and S-rich metallic liquid (12.5 wt% S in the core).

An improved estimate for the size and composition of the Martian core can be obtained by combining the Fe mass balance approach of Wänke and Dreibus (1988) with a trace element model similar to that used by Treiman et al. (1987). A new constraint is provided by our experimental determination of the partitioning behavior of Cu, a strongly chalcophile element whose abundance in the SPB mantle should be diagnostic of the S content of the core. Depletion factors were calculated for the moderately siderophile elements using the SPB mantle abundance estimates of Laul et al. (1986) (La) and of Wänke and Dreibus (1988) (Cr, Mn, Ni, Co, Cu). The metal-to-sulfide ratio of the core-forming material and the ambient f_{O_2}/f_{S_2} conditions during core formation were taken as independent variables in the model to determine whether a reasonable match to the inferred mantle siderophile element depletions could be achieved.

First, broad constraints were placed on Martian core formation by modeling the abundances of Co, Ni, and Cu at the most oxidizing conditions compatible with metal segregation (the IW buffer). The log f_{S_2} conditions were arbitrarily set at -2.0 (at 1350°C) as a starting point. The best match to the SPB mantle depletions for Co, Ni, and Cu was achieved with a core that is between 20.2 and 25.9% of the mass of Mars, containing only a small amount of S (~0.4 wt%). The extent of silicate partial melting accompanying core formation inferred from this model is relatively low (0.2 to 4.9 wt%). Models involving the segregation of S-rich material (14 to 35 wt% S) permit only a small core (5 to 9 wt%) and require large extents of silicate partial melting (60 to 78%) in order to match the Ni and Cu depletions. These models do not reproduce the Co depletion. Varying the ambient f_{O_2}/f_{S_2} conditions does not significantly affect this result.

The preliminary estimates for the size and composition of the Martian core derived from modeling trace element depletions were refined by assuming a chondritic Fe/La ratio for Mars and mass-balancing Fe between mantle and core using f_{O_2}/f_{S_2}-dependent partition coefficients. Mantle/core partition coefficients were calculated for each of the elements assumed to be in the core (Fe, Ni, Co, and Cu) using Eqn. 8. The mantle/core partition coefficient for Fe was modified by scaling the olivine/core partition coefficient to account for the presence of orthopyroxene and clinopyroxene using the SPB mantle mode of Longhi et al. (1992) and olivine/pyroxene partition coefficients determined from a Kilbourne Hole spinel lherzolite xenolith (Gaetani, 1996). The mantle/core partition coefficients were then used to calculate the concentration of each of the elements in the Martian core from their mantle abundance. When the core composition summed to less than 100%, it was recalculated at a lower f_{O_2} value until the appropriate core composition was obtained (Fig. 10; Table 13). The f_{O_2} conditions during core formation indicated by these calculations correspond to 0.53 log units below the IW buffer, with a core representing between 16.7% and 21.6% of the mass of Mars. The extent of silicate partial melting accompanying core formation implied by this model is 1.7 to 6.9%. Due to the low S content of the segre-

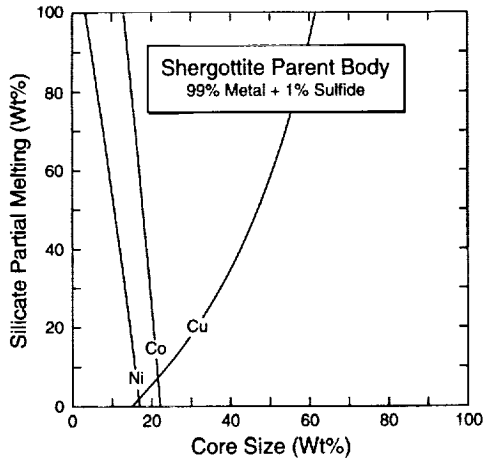

Fig. 10. Plot of core mass versus extent of silicate partial melting that accompanied segregation of a low-S core showing the modeling results for Co, Ni, and Cu depletions in the Martian mantle. Core formation f_{O_2}/f_{S_2} conditions tested in this model are log f_{O_2} = −10.73 and log f_{S_2} = −2.0 at 1350°C.

gating material, the calculations are insensitive to assumptions about f_{S_2} conditions.

Although the f_{O_2}/f_{S_2} dependence of the partitioning of W between sulfide melt and silicate melt could not be determined from our experiments, there is enough partitioning data available to perform a first-order test of whether the depletion of W in the SPB mantle is consistent with our proposed core formation model. Using the f_{O_2}-dependent metal/silicate melt partition coefficient for W of Schmidt et al. (1989) and our determination of the sulfide melt/silicate melt partition coefficient near IW, we found that the W abundance in the SPB mantle is consistent with the core mass inferred from the other elements if the percentage of sulfide in the segregating material is increased slightly to ~5% (1.8% S in the core) and the extent of silicate partial melting is increased to ~30 wt%.

There is no estimate for the V depletion of the SPB mantle and the depletion factors for Cr and Mn are both 1, so that their abundances cannot be modeled in the same way as Ni, Co, Cu, and W. However, the lack of any significant depletion for these elements in the SPB mantle can be used to test our proposed core formation model if Eqn. 9 is rearranged to solve for the depletion factor using the mean core size (19.2 wt%) and melt fraction (4.3%) obtained from our modeling results for Fe, Co, Ni, and Cu. The depletion factors for Cr and Mn calculated in this way are 1.08 and 1.01, respectively, consistent with the abundances inferred from SNC meteorites. Models involving segregation of sulfide-rich material (50–100% sulfide melt) produce significant depletions in both Cr (a = 1.97–2.88) and Mn (a = 1.18–1.36) in the SPB mantle. Therefore, our modeling results demonstrate that the segregation of metal-rich, S-poor material at low pressures and temperatures to form the Martian core is consistent with existing estimates for the concentrations of seven of the moderately siderophile elements in the SPB mantle.

Table 13, which is modified after Table 1 of Longhi et al. (1992), is a comparison of the SPB core composition calculated in this study with previous estimates. Core compositions 1–5 are based on cosmochemical models, while composition 6 is derived from Fe mass-balance. All of the existing models predict a Martian core with a significantly higher S content than our composition. The low S content of the Martian core implied by our modeling results has important implications for our understanding of the internal structure of Mars and for its early evolution. First, thermal models demonstrate that a core consisting dominantly of FeNi metal in a planet the size and age of Mars would be solid (Schubert and Spohn, 1990). A solid core is consistent with the lack of any significant magnetic field associated with Mars (Russell, 1978). The low S content of the core also implies that Mars is strongly depleted in S. With the exception of Morgan and Anders (1979), whose model core composition contains only 3.5 wt% S, all of the previous studies concluded that Mars is enriched with respect to S relative to the Earth. If the solubility of S in a silicate melt is taken to be 1500 ppm, the S/La ratio of Mars would be only 0.0065 times chondritic. This contrasts sharply with the elevated Martian volatile abundances inferred from studies of SNC meteorites (Dreibus and Wänke, 1987), but is consistent with the noble gas depletions observed in the Martian atmosphere (Anders and Owen, 1977; Owen et al., 1977). There are two possible explanations for a depletion in S. The first is that S was efficiently outgassed from the Martian interior during the early evolution of the planet. Once outgassed, S may have escaped from Mars along with the noble gases during the loss of a primordial atmosphere (Dreibus and Wänke, 1985). A second possibility is that the behavior of S during condensation of the solar nebula and accretion of the terrestrial planets is more complicated than currently assumed.

Acknowledgments—The authors would like to thank C. Capobianco, J. Jones, and E. Mathez for thorough and constructive reviews. We are also grateful to S. Bowring, F. Frey, P. Hess, and G. Hirth for their comments on the manuscript and to B. Z. Hanson for discussions on the geochemical behavior of chromium. The assistance of M. Jercinovic with the trace element determinations and image analyses was invaluable. This research was supported by NASA grant NAGW-3586 and an O.K. Earl Prize Postdoctoral Fellowship from the Division of Geological and Planetary Sciences at the California Institute of Technology.

Editorial handling: H. E. Newsom

REFERENCES

Abraham K. P. and Richardson F. D. (1960) Sulfide capacities of silicate melts. Part II. *J. Iron Steel Inst.* **196,** 313–317.

Abraham K. P., Davies M. W., and Richardson F. D. (1960) Sulfide capacities of silicate melts. Part I. *J. Iron Steel Inst.* **196,** 309–312.

Akella J., Williams R. J., and Mullins O. (1976) Solubility of Cr, Ti, and Al in co-existing olivine, spinel, and liquid at 1 atm. *Proc. 7th Lunar Planet. Sci. Conf.*, 1179–1194.

Anders E. and Grevesse N. (1989) Abundances of the elements: Meteoritic and solar. *Geochim. Cosmochim. Acta* **53,** 197–214.

Anders E. and Owen T. (1977) Mars and Earth: Origin and abundance of volatiles. *Science* **198,** 453–465.

Anderson D. L. (1972) Internal constitution of Mars. *J. Geophys. Res.* **77,** 789–795.

Barnes S. J. (1986) The distribution of chromium among orthopy-

roxene, spinel, and silicate liquid at atmospheric pressure. *Geochim. Cosmochim. Acta* **50,** 1889–1909.
Biggar G. M. (1972) Diopside, lithium metasilicate and the 1968 temperature scale. *Mineral. Mag.* **38,** 768–770.
Bills B. G. (1996) Geophysical constraints on the deep interior of Mars: Present status and future prospects (abstr.). *Lunar Planet. Sci.* **27,** 115–116.
Bills B. G. and Ferrari A. J. (1978) Mars topography harmonics and geophysical implications. *J. Geophys. Res.* **83,** 3497–3508.
Birch F. (1961) Composition of the Earth's mantle. *Geophys. J. R. Astron. Soc.* **4,** 295–311.
Birch F. (1964) Density and composition of mantle and core. *J. Geophys. Res.* **69,** 4377–4388.
Bogard D. D. and Johnson P. (1983) Martian gases in an Antarctic meteorite. *Science* **221,** 651–654.
Borisov A. and Palme H. (1995) The solubility of iridium in silicate melts: New data from experiments with $Ir_{10}Pt_{90}$ alloys. *Geochim. Cosmochim. Acta* **59,** 481–485.
Bottinga Y. and Weill D. F. (1972) The viscosity of magmatic silicate liquids: A model for calculation. *Amer. J. Sci.* **272,** 438–475.
Brett R. (1984) Chemical equilibration of the Earth's core and upper mantle. *Geochim. Cosmochim. Acta* **48,** 1183–1188.
Capobianco C. J. and Amelin A. A. (1994) Metal-silicate partitioning of nickel and cobalt: The influence of temperature and oxygen fugacity. *Geochim. Cosmochim. Acta* **58,** 125–140.
Chase M. W., Jr., Davies C. A., Downey J. R., Jr., Frurip D. J., McDonald R. A., and Syverud A. N. (1985) JANAF Thermochemical Tables, 3rd ed. *J. Phys. Chem. Ref. Data* **14,** Suppl. 1, Part I, Al-Co, Part II, Cr-Zr.
Drake M. J., Newsom H. E., and Capobianco C. J. (1989) V, Cr, and Mn in the Earth, Moon, EPB, and SPB and the origin of the Moon: Experimental studies. *Geochim. Cosmochim. Acta* **53,** 2101–2111.
Dreibus G. and Wänke H. (1985) Mars, a volatile-rich planet. *Meteoritics* **20,** 367–381.
Dreibus G. and Wänke H. (1987) Volatiles on Earth and Mars: A comparison. *Icarus* **71,** 225–240.
Ehlers K., Grove T. L., Sisson T. W., Recca S. I., and Zervas D. A. (1992) The effect of oxygen fugacity on the partitioning of nickel and cobalt between olivine, silicate melt, and metal. *Geochim. Cosmochim. Acta* **56,** 3733–3743.
Fincham C. J. B. and Richardson F. D. (1954) The behavior of sulfur in silicate and aluminate melts. *Phil. Trans. Roy. Soc. London* **223,** 40–62.
Gaetani G. A. (1996) Experimental Investigations of Differentiation Processes in the Terrestrial Planets. Ph.D. diss., Massachusetts Institute of Technology.
Goettel K. A. (1983) Present constraints on composition of the mantle of Mars. *Carnegie Inst. Wash. Yearbk* **82,** 363–366.
Grossman L. (1972) Condensation in the primitive solar nebula. *Geochim. Cosmochim. Acta* **36,** 597–619.
Hanson B. Z., Jones J. H., and Gaetani G. A. (1996) Partition coefficients for Cr^{2+} and Cr^{3+} between olivine and liquid are virtually identical: Cr and V partitioning among olivine, spinel, and silicate liquid over a wide range of f_{O2}'s (abstr.). *Eos; Trans. Amer. Geophys. Union* **77,** 846–847.
Hart S. R. and Davis K. (1978) Nickel partitioning between olivine and silicate melt. *Earth Planet. Sci. Lett.* **40,** 203–219.
Haughton D., Roeder P. L., and Skinner B. J. (1974) Solubility of sulfur in mafic magmas. *Econ. Geol.* **69,** 451–467.
Hillgren V. J., Drake M. J., and Rubie D. C. (1994) High-pressure and high-temperature experiments on core-mantle segregation in the accreting Earth. *Science* **264,** 1442–1445.
Hillgren V. J., Drake M. J., and Rubie D. C. (1996) High pressure and high temperature metal-silicate partitioning of siderophile elements: The importance of silicate liquid composition. *Geochim. Cosmochim. Acta* **60,** 2257–2263.
Hirschmann M. M. and Ghiorso M. S. (1994) Activities of nickel, cobalt, and manganese silicates in magmatic liquids and applications to olivine/liquid and to silicate/metal partitioning. *Geochim. Cosmochim. Acta* **58,** 4109–4126.
Holzheid A., Borisov A., and Palme H. (1994) The effect of oxygen fugacity and temperature on solubilities of nickel, cobalt, and molybdenum in silicate melts. *Geochim. Cosmochim. Acta* **58,** 1975–1981.
Huebner J. S., Lipin B. R., and Wiggins L. B. (1976) Partitioning of chromium between silicate crystals and melts. *Proc. 7th Lunar Planet. Sci. Conf.,* 1195–1220.
Jagoutz E. et al. (1979) The abundances of major, minor and trace elements in the earth's mantle as derived from primitive ultramafic nodules. *Proc. 10th Lunar Planet. Sci. Conf.,* 2031–2050.
Jones J. H. and Drake M. J. (1983) Experimental investigations of trace element fractionation in iron meteorites, II: The influence of sulfur. *Geochim. Cosmochim. Acta* **47,** 1199–1209.
Jones J. H. and Drake M. J. (1986) Geochemical constraints on core formation in the Earth. *Nature* **322,** 221–228.
Jones J. H. and Walker D. (1991) Partitioning of siderophile elements in the Fe-Ni-S system: 1 bar to 80 kbar. *Earth Planet. Sci. Lett.* **105,** 127–133.
Keppler H. and Rubie D. (1993) Pressure-induced coordination changes of transition-metal ions in silicate melts. *Nature* **364,** 54–56.
Kinzler R. J. and Grove T. L. (1985) Crystallization and differentiation of Archean komatiite lavas from northeast Ontario: Phase equilibrium and kinetic studies. *Amer. Mineral.* **70,** 40–51.
Kinzler R. J., Grove T. L., and Recca S. I. (1990) An experimental study of the effect of temperature and melt composition on the partitioning of nickel between olivine and silicate melt. *Geochim. Cosmochim. Acta* **54,** 1255–1265.
Laul J. C. et al. (1986) Chemical systematics of the Shergotty meteorite and the composition of its parent body (Mars). *Geochim. Cosmochim. Acta* **50,** 909–926.
Lewis J. S. (1972) Metal/silicate fractionation in the solar system. *Earth Planet. Sci. Lett.* **15,** 286–290.
Li J. and Agee C. B. (1996) Geochemistry of mantle-core differentiation at high pressure. *Nature* **381,** 686–689.
Longhi J., Knittle E., Holloway J. R., and Wänke H. (1992) The bulk composition, mineralogy and internal structure of Mars. In *Mars* (ed. H. H. Kieffer et al.), pp. 184–212. University of Arizona Press.
McMillan P. F. and Kirkpatrick R. J. (1992) Al coordination in magnesium aluminosilicate glasses. *Amer. Mineral.* **77,** 898–900.
McSween H. Y., Jr. et al. (1979) Petrogenetic relationship between Allan Hills 77005 and other achondrites. *Earth Planet. Sci. Lett.* **45,** 275–284.
Mikouchi T., McKay G., and Le L. (1994) Cr, Mn and Ca distributions for olivine in Angritic systems: Constraints on the origins of Cr-rich and Ca-poor core olivine in Angrite LEW87051 (abstr.). *Lunar Planet. Sci.* **25,** 907–908.
Morgan J. W. and Anders E. (1979) Chemical composition of Mars. *Geochim. Cosmochim. Acta* **43,** 1601–1610.
Morgan J. W., Wandless G. A., Petrie R. K., and Irving A. J. (1980) Composition of the Earth's upper mantle—II: Volatile trace elements in ultramafic xenoliths. *Proc. 11th Lunar Planet. Sci. Conf.,* 213–233.
Murck B. W. and Campbell I. H. (1986) The effects of temperature, oxygen fugacity, and melt composition on the behavior of chromium in basic and ultrabasic melts. *Geochim. Cosmochim. Acta* **50,** 1871–1887.
Murthy V. R. (1991) Early differentiation of the Earth and the problem of mantle siderophile elements: A new approach. *Science* **253,** 303–306.
Newsom H. E. (1985) Molybdenum in Eucrites: Evidence for a metal core in the Eucrite parent body. *Proc. 15th Lunar Planet. Sci. Conf.,* C613–C617.
Newsom H. E. (1990) Accretion and core formation in the Earth: Evidence from siderophile elements. In *Origin of the Earth* (ed. H. E. Newsom and J. H. Jones), pp. 273–288. Oxford University Press.
Nisbet E. G. and Walker D. (1982) Komatiites and the structure of the Archean mantle. *Earth Planet. Sci. Lett.* **60,** 105–113.
Owen T., Biemann K., Rushneck D. R., Biller J. E., Howarth D. W., and LaFleur A. L. (1977) The composition of the atmosphere at the surface of Mars. *J. Geophys. Res.* **82,** 4635–4639.
Peach C. L. and Mathez E. A. (1993) Sulfide melt-silicate melt distribution coefficients for nickel and iron and implications for the

distribution of other chalcophile elements. *Geochim. Cosmochim. Acta* **57,** 3013–3021.

Poirier J. (1994) Light elements in the Earth's outer core: A critical review. *Physics Earth Planet. Int.* **85,** 319–337.

Rajamani V. and Naldrett A. J. (1978) Partitioning of Fe, Co, Ni, and Cu between sulfide liquid and basaltic melts and the composition of Ni-Cu sulfide deposits. *Econ. Geol.* **73,** 82–93.

Rammensee W. and Wänke H. (1977) On the partition coefficient of tungsten between metal and silicate and its bearing on the origin of the moon. *Proc. 8th Lunar Planet. Sci. Conf.,* 399–409.

Ringwood A. E. (1966) Chemical evolution of the terrestrial planets. *Geochim. Cosmochim. Acta* **30,** 41–104.

Ringwood A. E. (1981) The Canberra Model of planet formation. In *Basaltic Volcanism on the Terrestrial Planets,* pp. 653–656. Pergamon.

Roeder P. L. and Reynolds I. (1991) Crystallization of chromite and chromium solubility in basaltic melts. *J. Petrol.* **32,** 909–934.

Russell C. T. (1978) The magnetic field of Mars: Mars 5 evidence re-examined. *Geophys. Res. Lett.* **5,** 85–88.

Schmidt W., Palme H., and Wänke H. (1989) Experimental determination of metal/silicate partition coefficients for P, Co, Ni, Cu, Ga, Ge, Mo, and W and some implications for the early evolution of the Earth. *Geochim. Cosmochim. Acta* **53,** 173–185.

Schreiber H. D. and Haskin L. A. (1976) Chromium in basalts: Experimental determination of redox states and partitioning among synthetic silicate phases. *Proc. 7th Lunar Planet. Sci. Conf.,* 1221–1259.

Schubert G. and Spohn T. (1990) Thermal history of Mars and the sulfur content of its core. *J. Geophys. Res.* **95,** 14095–14104.

Seifert S. and Ringwood A. E. (1988) The lunar geochemistry of chromium and vanadium. *Earth, Moon, and Planets* **40,** 45–70.

Shimizu N. and Hart S. R. (1982) Applications of the ion microprobe to geochemistry and cosmochemistry. *Ann. Rev. Earth Planet. Sci.* **10,** 483–526.

Stolper E. M. (1979) Trace elements in shergottite meteorites: Implications for the origin of planets. *Earth Planet. Sci. Lett.* **42,** 239–242.

Stolper E. M. and McSween H. Y., Jr. (1979) Petrology and origin of the shergottite meteorites. *Geochim. Cosmochim. Acta* **43,** 1475–1498.

Surkov Y. A. (1977) *Gamma Spectrometry in Cosmic Investigations.* Atomizdat.

Thibault Y. and Walter M. J. (1995) The influence of pressure and temperature on the metal-silicate partition coefficients of nickel and cobalt in a model C1 chondrite and implications for metal segregation in a deep magma ocean. *Geochim. Cosmochim. Acta* **59,** 991–1002.

Treiman A. H., Drake M. J., Janssens M., Wolf R., and Ebihara M. (1986) Core formation in the Earth and Shergottite Parent Body (SPB): Chemical evidence from basalts. *Geochim. Cosmochim. Acta* **50,** 1071–1091.

Treiman A. H., Jones J. H., and Drake M. J. (1987) Core formation in the Shergottite parent body and comparison with the Earth. *J. Geophys. Res.* **92,** E627–E632.

Walker D., Stolper E. M., and Hayes J. F. (1979) Basaltic volcanism: The importance of planet size. *Proc. 10th Lunar Planet. Sci. Conf.,* 1995–2015.

Walker D., Norby L., and Jones J. H. (1993) Superheating effects on metal-silicate partitioning of siderophile elements. *Science* **262,** 1858–1861.

Wänke H. (1981) Constitution of the terrestrial planets. *Phil. Trans. Roy. Soc. London* **A303,** 287–302.

Wänke H. and Dreibus G. (1988) Chemical composition and accretionary history of the terrestrial planets. *Phil. Trans. Roy. Soc. London* **A325,** 545–557.

Weidenschilling S. J. (1976) Accretion of the terrestrial planets. II. *Icarus* **2,** 161–170.

White W. B., Johnson S. M., and Dantzig G. B. (1958) Chemical equilibrium in complex mixtures. *J. Chem. Phys.* **28,** 751–755.